AGU PUBLICATIONS

Tectonics

RESEARCH ARTICLE
10.1002/2017TC004686

Key Points:
- We present a methodology for reverse-engineering subducted slabs to their presubduction geometries by modeling them as viscoelastic sheets
- This method tests the viability of slab models, showing where tears are required to allow inferred slabs to adopt their current morphologies
- Reverse-engineering the Ryukyu and Shikoku slabs demonstrates that they tore open along the subducted Kyushu-Palau and Gagua ridges

Supporting Information:
- Supporting Information S1
- Movie S1
- Movie S2
- Movie S3
- Movie S4
- Movie S5
- Movie S6
- Movie S7
- Movie S8
- Movie S9

Correspondence to:
J. M. Pownall,
jonathan.pownall@anu.edu.au

Citation:
Pownall, J. M., G. S. Lister, and W. Spakman (2017), Reconstructing subducted oceanic lithosphere by "reverse-engineering" slab geometries: The northern Philippine Sea Plate, *Tectonics*, *36*, 1814–1834, doi:10.1002/2017TC004686.

Received 12 JUN 2017
Accepted 10 AUG 2017
Accepted article online 23 AUG 2017
Published online 18 SEP 2017

Reconstructing subducted oceanic lithosphere by "reverse-engineering" slab geometries: The northern Philippine Sea Plate

Jonathan M. Pownall[1], Gordon S. Lister[1], and Wim Spakman[2,3]

[1]Research School of Earth Sciences, Australian National University, Canberra, ACT, Australia, [2]Department of Earth Sciences, Utrecht University, Utrecht, Netherlands, [3]Center for Earth Evolution and Dynamics (CEED), University of Oslo, Oslo, Norway

Abstract Subducting slabs commonly acquire complex geometries from the migration of subduction trenches, slab-mantle interaction, slab tearing, and collision of slabs at depth. Although it is possible to construct three-dimensional models of subducted slabs using earthquake hypocenter locations and tomographic models, it is often not possible to rigorously test their accuracy. Here we present a methodology for performing such a test, by "reverse-engineering" the presubduction configuration of a slab of oceanic lithosphere from interpretations of its present-day morphology. We illustrate our approach for the Ryukyu and Shikoku slabs, northwest Philippine Sea, having simulated them as viscoelastic sheets that we unfolded and "floated" to the surface. The net strain distribution of the floated mesh indicated which parts of the original slab model were geometrically viable (minimal net strain) and which parts of the mesh required additional tears and/or zones of localized ductile extension to have enabled the slab to deform during subduction. In the instance of the Ryukyu and Shikoku slabs, the Palau-Kyushu and Gagua ridges are shown to have both acted as planes of weakness that broke into major vertical slab tears. These subducted ridges are connected by a trench-parallel tear that represented the former contact between the Huatung and West Philippine Basins. The fossil spreading center of the Shikoku Basin formed a separate slab window upon subduction along the Nankai Trough. The methodology presented herein is a powerful tool to evaluate complex slab morphologies, infer the locations of slab tears, and therefore reconstruct intricate configurations of subducted oceanic lithosphere.

Plain Language Summary When a plate enters a subduction zone, it is often crumpled by its interaction with the Earth's mantle and other subducting plates. Although it is possible to infer the approximate shape of these subducted slabs from the locations of earthquakes that they produce, it is often not possible to test how accurate these inferences are. Here we present a way to test whether a given slab model could have realistically been attained from crumpling a subducting plate by a process of "reverse-engineering." Using a computer program, we simulate the crumpled and ripped slabs as rubber-like sheets that we unfold and "float" to the Earth's surface. If the modeled slab can float up and unfold without undergoing much of a change to its surface area, then it is shown to have a plausible geometry. But if a slab model cannot easily unfold, then the methodology shows where additional rips and tears were required to have enabled the slab to deform during its subduction. This methodology is a powerful tool to both evaluate the viability of complex subduction zone models and to therefore produce reconstructions of subducted oceanic plates. This approach here reveals large tears in subducted slabs beneath SW Japan.

1. Introduction

Seismicity and seismic tomography in particular have unveiled the fate of subducted oceanic lithosphere in increasing detail, leading to various inferences of complex slab morphology. A subducting slab will bend, fold, rip, stretch, tear, or detach [*Wortel and Spakman*, 2000; *Spakman and Wortel*, 2004; *Lister et al.*, 2008, 2012; *Rosenbaum et al.*, 2008; *Sigloch et al.*, 2008; *Obayashi et al.*, 2009; *van Hunen and Allen*, 2011] in response to changes in trench location and geometry [*Spakman and Hall*, 2010; *Lister et al.*, 2012], the influence of pre-existing slab structures [*Thorkelson*, 1996], interactions with surrounding mantle [*Spakman and Hall*, 2010; *Chertova et al.*, 2014; *Sternai et al.*, 2014], collision of slabs at depth [*Richards et al.*, 2011], and the geometrical

consequences of subducting into a spherical Earth [*Miller et al.*, 2006; *Lister et al.*, 2012]. Consequently, the morphologies adopted by slabs are often complex. Understanding how slab morphology has been influenced by these processes is critical in reconstructing subducted oceans, understanding the precursors to continental collision, and therefore in producing continent-scale plate reconstructions [*van Hinsbergen et al.*, 2012; *Hall and Spakman*, 2015; *Wu et al.*, 2016].

Conceptually, tears in a slab will develop preferentially along zones of weakness inherited from subducted arcs, spreading centers, transform faults, fracture zones, and other ridges that developed in the oceanic lithosphere before it was subducted. A problem, however, is that associated slab morphology change or tears are often difficult to interpret directly from the available geophysical data sets (seismicity and tomographic models), especially if the window created by the tear is narrow or if the tear enables two parts of a slab to closely overlap. Furthermore, interpreting tomographic models directly depends clearly on the quality of the tomographic image, which is often also difficult to assess [e.g., *Rawlinson and Spakman*, 2016].

One alternative way of understanding how slab morphology and tearing evolves is by forward numerical modeling, preferably using initial and boundary conditions that mimic the natural setting closely [e.g., *Moresi et al.*, 2014; *Chertova et al.*, 2014]. Another way is to assess the length of subducted slabs from earthquakes and/or seismic tomography, before "unfolding" them to the surface [e.g., *Ansell and Adams*, 1986; *Chatelain et al.*, 1993; *Wu and Suppe*, 2011; *Wu et al.*, 2016]. However, this latter method often requires subjective judgements as to the length of slab represented by broad or poorly resolved *P* wave anomalies. A better methodology would incorporate rigorous testing of different slab models that are permitted by the best available, but often suboptimal, data.

Here we develop a method to test the viability of an interpreted slab geometry, to assess whether it was ever possible for an oceanic shell, upon being subducted, to have been deformed into its alleged shape. This test can be performed, quantitatively, using numerical simulation to mathematically "unfold" a complex slab model into its presubducted configuration—a procedure we refer to here as "reverse-engineering." In this paper, we implement a new approach to test the viability of an interpreted slab geometry, developed and first presented in an earlier form by *Lister et al.* [2012] using the Mac OS software *Pplates* [*Lister*, 2017a]. A fortunate consequence of this reverse-engineering approach is that the process of "floating" may successfully flag parts of the mesh that are required to have been torn in order that the slab achieved its hypothesized shape.

For illustrative purposes, the specific examples chosen here are the Ryukyu and Shikoku slabs [*Lallemand et al.*, 1997; *Chou et al.*, 2006; *Nakajima and Hasegawa*, 2007; *Wu et al.*, 2009; *Hsu et al.*, 2013] that subduct to the northwest from the Philippine Sea between Taiwan and Japan (Figure 1). These slabs are extensively studied, exhibit moderate complexity within a relatively compact size, and have been modeled and reconstructed by previous studies [*Lallemand et al.*, 2001; *Zhao et al.*, 2012; *Huang et al.*, 2013; *Wei et al.*, 2015; *Wu et al.*, 2016; *Lallemand*, 2016].

2. The Philippine Sea and the Ryukyu and Shikoku Slabs

The Philippine Sea plate comprises several oceanic basins of different ages and spreading histories bound by multiple subduction zones (Figure 1). The plate subducts both northwest along the Ryukyu Trench and the Nankai, Suruga, and Sagami troughs; and to the west at the Philippine Trench. Along its eastern boundary, the Philippine Sea is the upper plate to the Pacific and Caroline Sea plates, which subduct westward along the Izu-Bonin, Mariana, Yap, and Palau trenches. The South China Sea also subducts beneath the Philippine Sea plate, eastward along the Manila Trench. The short slow-spreading Ayu Trough [*Fujiwara et al.*, 1995] connecting the south Philippine Sea Plate to the Caroline Sea is the only divergent boundary.

The oldest part of the Philippine Sea plate is the West Philippine Basin, which began to open from 54 Ma [*Deschamps and Lallemand*, 2002] along its E-W trending Central Basin Fault Rift system [*Mrozowski et al.*, 1982; *Hilde and Lee*, 1984; *Hall et al.*, 1995a, 1995b; *Deschamps and Lallemand*, 2002; *Lallemand*, 2016]. During the early stages of this rifting, the Pacific Plate began to subduct under the West Philippine Basin's eastern margin—a subduction zone that would later evolve into the Izu-Bonin-Mariana system. After the West Philippine Basin had ceased spreading at approximately 33–30 Ma [*Deschamps and Lallemand*, 2002], eastward rollback of the Izu-Bonin and Mariana slabs extended back-arc regions, caused part of the original volcanic arc—now termed the Kyushu-Palau Ridge—to rift away from the active Izu-Bonin-Mariana arcs. This caused the initiation of a new N-S trending oceanic spreading center, which opened the southern Parece Vela

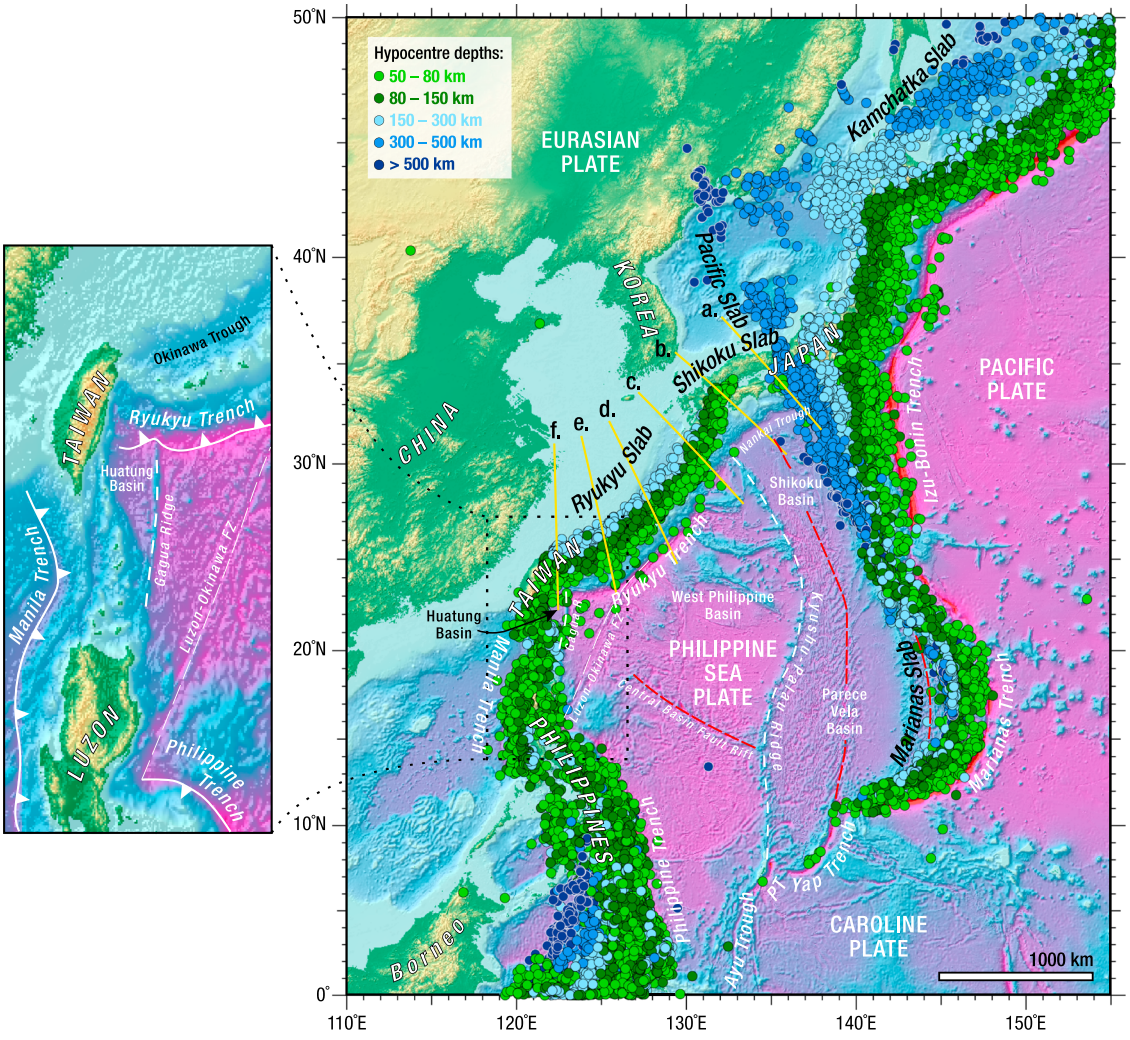

Figure 1. Map of the Philippine Sea and surrounding regions. Colored dots show the locations of earthquake hypocenters (projected to surface level) catalogued by the *International Seismological Centre* [2016] for earthquakes of magnitude 4 and greater that occurred between 1 January 2000 and 1 January 2016. Hypocenters are colored by depth: light green—50–80 km; dark green—80–150 km; light blue—150–300 km; mid blue—300–500 km; and dark blue—>500 km. Hypocenters shallower than 50 km depth, and those with unknown depth locations, have been omitted for clarity. Yellow lines show the locations of cross-sections a–f shown in Figure 2. Enlargement (left) shows the setting of the Huatung Basin. Basemap bathymetry data are from *Ryan et al.* [2009]. R—Ridge; FZ—Fracture Zone; and PT—Palau Trench.

basin from 29 Ma [*Okino et al.*, 1998] and the northern Shikoku basin from 25 Ma [*Okino et al.*, 1994], both ceasing at 15 Ma during a major regional plate reconfiguration event [*Sibuet et al.*, 2002; *Sdrolias et al.*, 2004]. Rifting of these basins was accompanied by clockwise rotation of the Philippine Sea Plate from 25 Ma [*Hall et al.*, 1995a] or 20 Ma [*Sdrolias et al.*, 2004], after which from approximately 15 Ma the northern margin was subducted along the Ryukyu Trench and Nankai Trough [*Mahony et al.*, 2011]. Rollback of the Mariana slab, which began just prior to 5 Ma [*Yamazaki et al.*, 2003], continues to open the Mariana Trough.

At present, the Kyushu-Palau Ridge represents a topographically prominent, curved aseismic "remnant arc" [*Karig*, 1972] that bisects the Philippine Sea, separating those younger approximately 29–15 Ma) eastern extended back-arc basins from the older (approximately 54–30 Ma) West Philippine Basin (Figure 1). Along the northwestern edge of the West Philippine Basin is the short Gagua Ridge, rising 4 km above the ocean floor and trapping the small Huatung Basin to its west against Taiwan [*Schnürle et al.*, 1998; *Kuo et al.*, 2009; *Eakin et al.*, 2015]. This ridge is thought to be a former fracture zone [*Mrozowski et al.*, 1982; *Hilde and Lee*, 1984; *Deschamps et al.*, 1998] that operated either in the Oligocene [*Deschamps and Lallemand*, 2002] or Miocene [*Eakin et al.*, 2015] as a site of West Philippine Basin underthrusting and so represents a "failed" subduction zone [*Deschamps et al.*, 1998; *Deschamps and Lallemand*, 2002; *Eakin et al.*, 2015]. Although initially thought

to be part of the West Philippine Basin [*Hilde and Lee*, 1984], the Huatung Basin is now considered to be of a different origin (and possibly different plate) [*Deschamps et al.*, 1998; *Eakin et al.*, 2015], but age estimates by different authors vary considerably between 140 Ma [*Lallemand et al.*, 2013], 131–119 Ma [*Deschamps et al.*, 2000], 51–43 Ma [*Sibuet et al.*, 2002], 42–33 Ma [*Doo et al.*, 2015], 35 Ma [*Gutscher et al.*, 2016], and 30–15 Ma [*Kuo et al.*, 2009]. As such, the nature and thermal history of the Huatung lithosphere remains elusive [*Gutscher et al.*, 2016]—is it younger than the West Philippine Basin or does it represent a trapped fragment of Early Cretaceous oceanic lithosphere?

Cross-cutting the West Philippine Basin slightly farther east is the left-lateral Luzon-Okinawa Fracture Zone, which closely parallels and then is obliquely subducted along Ryukyu Trench toward its eastern extent [*Hsu et al.*, 2013]. According to *Lallemand* [2016], this feature may have accommodated a few hundreds of kilometers of displacement, although its exact role in the development of the West Philippine Basin, and its influence on the subducted part of the lithosphere, is not fully understood.

Convergence across the Ryukyu Trench occurs today at a rate of 80–88 mm a^{-1} (ESE-WNW direction) [*DeMets et al.*, 2010], with active extension of the Okinawa Trough back-arc basin having decoupled the motion of the Ryukyu forearc from Eurasia [*Nakamura*, 2004]. A considerable portion of the Philippine Sea Plate has been subducted beneath Eurasia, starting at approximately 48 Ma [*Seno and Maruyama*, 1984], and later occurring specifically along the Ryukyu Trench from approximately 25 to 15 Ma until present [*Hall*, 2002; *Sibuet et al.*, 2002]. An arcuate curtain of seismicity defines the Ryukyu and Shikoku slabs, dipping ~45° to the NW down to ~250 km depth; but below this depth, different interpretations have arisen from different tomographic models [*Bijwaard et al.*, 1998; *Widiyantoro et al.*, 1999; *Lallemand et al.*, 2001; *Wang et al.*, 2008; *Li and van der Hilst*, 2010; *Wei et al.*, 2012, 2015; *Zhao et al.*, 2012; *Huang et al.*, 2013; *Cao et al.*, 2014; *Gutscher et al.*, 2016; *Wu et al.*, 2016], detailed later in section 5.1.

3. Constructing a New Model for the Ryukyu Slab

We interpreted the geometry of the Ryukyu and Shikoku slab using two data sets: (i) earthquake hypocenter locations catalogued by the International Seismological Center (ISC) [*International Seismological Centre*, 2016] and (ii) the *P* wave tomographic model UU-P07 of *Amaru* [2007], described also by *Hall and Spakman* [2015], relative to the ak135 reference model of *Kennett et al.* [1995].

3.1. Assumptions

As earthquakes may nucleate in and propagate through all depths of the slab and the mantle wedge [e.g., *Davies*, 1999; *Peacock*, 2001], it is not yet possible to infer how seismicity exactly relates to the surface of any given slab. However, for the purposes of this study, in order to adopt a consistent interpretation method we make the assumption that the upper plane of seismicity always correlates with the slab-mantle wedge interface. We also make the assumption that a slab maintains a constant surface area upon subduction and therefore that all density increases (volume reductions) resulting from eclogitization and higher-pressure phase changes [e.g., *Aoki and Takahashi*, 2004] result only in decreases in slab thickness. The third main assumption is that all deformation is accommodated by folding and faulting (or ripping or tearing). Evidence for slab stretching and boudinage [*Lister et al.*, 2008] demonstrates that this third assumption cannot always hold true, but for the purposes of our slab floating methodology it does not matter; "tears" that feature in the final interpreted slab model may be interpreted with equal validity instead as zones of plastic extension or shortening. However, for clarity and brevity, we assume that folding and tearing are the only ways to accommodate deformation of what we describe as "rigid slabs."

3.2. Earthquake Hypocenter Interpretation

Earthquake hypocenters were analyzed using the Mac OS program *eQuakes* [*Lister*, 2017b] to produce a 3-D pointset bounding the upper plane of seismicity. This analysis was performed on earthquakes catalogued by the ISC of magnitude 4 or greater located between 110–155°E, 0–50°N, and 0–1000 km depth that occurred between January 2000 and October 2015 [*International Seismological Centre*, 2016]. Hypocenters with unknown depths were omitted.

eQuakes was used to produce three sets of ~300 closely spaced (< 10 km) cross sections through this data set oriented roughly perpendicular to the Ryukyu Trench and Nankai Trough. Each cross-section plane displayed a perpendicular projection of earthquake hypocenters located within 20 km either side (Figures 2a–2f); each set of cross sections covered the entire Ryukyu and Shikoku slabs (Figure S1); and each of the three sets of cross sections, relative to each other, had slightly different orientations so as to produce a cross-cutting lattice.

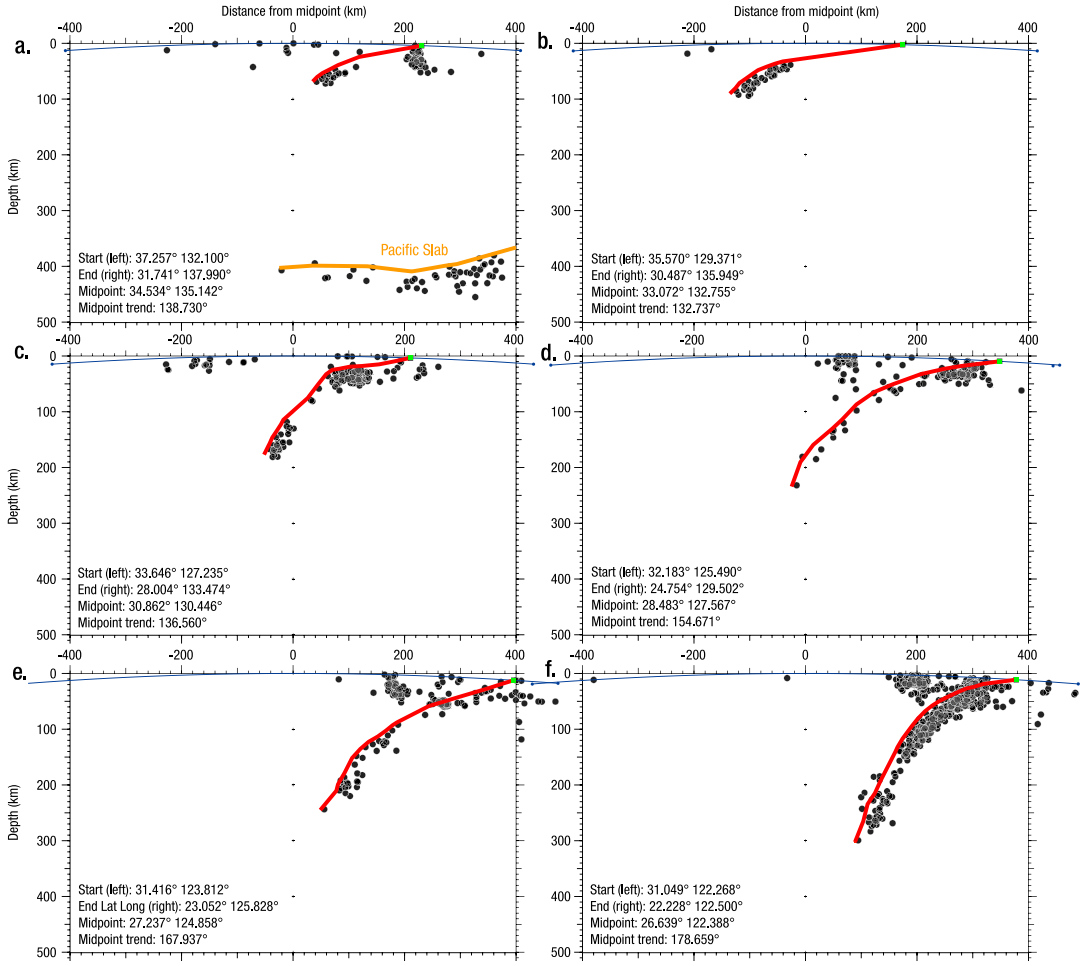

Figure 2. Cross sections through the seismicity associated with the Ryukyu and Shikoku slabs, as located by the yellow lines in Figure 1. The red lines show the interpretation for the upper plane of seismicity, which are extrapolated back to the location of the trench (depicted by the small green squares). Hundreds of interpretations like these (Figure S1) have been output into *GOCAD* to produce the slab mesh shown in Figure 5. The orange line in part (a) shows the upper plane of seismicity for the Pacific slab. Earthquakes are projected onto planes of sections from up to 20 km perpendicular distance. The "start" and "end" locations of each section (as annotated along the bottom of each plot) refers to the location of the blue dots at the ends of the blue lines showing the intersection between the planes of section and the Earth's surface. All figures producing using *eQuakes*.

This approach meant that each part of the slab's seismicity was interpreted three times, and the effect of any bias resulting from a particular orientation of cross section was minimized. Each cross section was interpreted manually by "drawing" a polyline along the upper plane of seismicity within *eQuakes* (Figure 2). The number of nodes defining this polyline for a given section (or part of section) was chosen to reflect the degree of confidence in the interpretation—for instances where a dense cluster of hypocenters are defined by a single sharp, unambiguous plane of seismicity, the interpretive polyline was defined by many nodes (i.e., at 5 or 10 km spacings); but in instances where the location of the upper plane of seismicity was ambiguous, only a small number of nodes were selected to define the plane. Importantly, aseismic regions (since they *could* represent holes or tears in the slab) were not interpreted as belonging to part of a slab. Variations in the resulting pointset densities therefore reflect the degree of confidence of the interpreter in the slab geometry at any given point.

This pointset was then exported (as an xyz .csv file) to the program *GOCAD*, where it was used to build a 3-D mesh of interconnected nodes, edges, and faces. This mesh was then edited to remove misinterpolations made by the mesh-building function in *GOCAD*, such as planes that were incorrectly built to bridge over aseismic gaps. A mild smoothing function (*GOCAD*'s "beautify triangles for equilaterality" operation) was then applied to remove roughness caused by minor, short-wavelength inconsistencies between each of the three sets of interpretations. Importantly, (i) the smoothing function only affected small-scale (<10 km scale)

features of the slab mesh and so critically did not affect its overall morphology and (ii) this smoothing operation did not affect the mesh density, and so the final edited mesh still reflected the original interpretation. Furthermore, application of this smoothing function was absolutely necessary to minimize the exaggeration to the surface area of the slab mesh caused by artificial roughness in the "raw" interpretation.

3.3. *P* wave Tomography Interpretation

The tomographic model UU-P07 (Movies S1–S4 in the supporting information) was loaded into the same *GOCAD* project where it was used to extend the slab mesh into aseismic regions and below the 660 km depth mantle discontinuity where no (/very few) earthquakes are generated (Figure 3). Individual E-W, N-S, and horizontal sections through the tomographic data set were interpreted sequentially, and then the nodes interpreted from this procedure were combined with parts of the mesh interpreted from the earthquake hypocenters. The smoothing procedure outlined earlier was only applied once the whole "raw" mesh had been constructed. Last of all, an oceanic "skirt" was built for the slab by appending a planar mesh representing the present-day ocean floor, extending southeast from the Ryukyu Trench to a distance of ~200 km. The approximation of modeling this ocean floor at zero meters depth is reasonable, considering that a typical ocean floor depth of ~3 km represents <0.5% of the distance to the 660 km transition zone.

A perfect correlation between the most positive *P* wave anomalies and the distribution of earthquake hypocenters should not be expected. These two data sets are nonequivalent. So our approach was to build a mesh that maps the upper plane of seismicity and utilizes the morphologies of positive *P* wave anomalies to extrapolate this trend to greater depth and lateral extent (Figure 4a). Our interpretation of the broader *P* wave anomalies led to a more conservative interpretation of the slab geometry at depth, which is evident from the markedly lower mesh density in these regions (Figure 5b). Although a few small-scale (<50 km) features interpreted from only the *P* wave tomography arguably fall within the uncertainty of the data, we can confirm that structures larger than 50–100 km are demonstrated by sensitivity tests (Movies S4–S6) [*Spakman and Nolet*, 1988; *Rawlinson and Spakman*, 2016] to be identifiable and sufficiently resolved spatially.

In order to be consistent in our interpretations, we adhered consistently to the following rules:

1. The upper plane of seismicity is interpreted as the top surface of the slab;
2. In instances where the hypocenter locations and most positive (fastest) *P* wave anomalies are in conflict, the seismicity is considered the most reliable indicator of the slab location (Figure 4a, point 2);
3. Aseismic regions that correlate with negative (slow) *P* wave anomalies should be interpreted as holes, gaps, rips, or tears in the slab if allowed by the attained spatial resolution. However, aseismic regions that correlate with positive (fast) *P* wave anomalies may indicate the occurrence of a slab;
4. No editing of the mesh (apart from the mild smoothing) should be performed on parts of the mesh interpreted from sharp planes of seismicity;
5. When using *P* wave tomography to interpret a slab in an aseismic region, the center of the fastest anomaly should be chosen (in the absence of other constraints); *but*
6. When using the *P* wave tomography to extend the slab mesh beyond the seismic parts of the slab, the trajectory of the slab should be maintained. That is, if the slab mesh interpreted from seismicity is misaligned with the most positive *P* wave anomaly, then the mesh should instead be extrapolated by running along whichever (lower) positive *P* wave anomaly value *is* aligned with the seismicity (Figure 4a, point 3); and
7. In instances where the positive (fast) *P* wave anomalies are broad, the simplest interpretation in the absence of other contraints should be made, so that the surface area of the final slab will always represent a minimum. While an interpretation that drapes back and forth across the extent of the anomaly is arguably permitted by the available data (Figure 4c, point 7), this approach likely leads to an overestimation of the original surface area of the slab.

3.4. The Initial Slab Model

The final slab mesh for the Ryukyu Slab (Figure 5) was exported as a .dxf file into the Mac OS program *Pplates* [*Lister*, 2017a]. This .dxf file was also used to build a 3-D .pdf file, which is available to be viewed in Figure S2.

We interpret a horizontal tear (we name the "Ryukyu Tear") between 250 and 350 km depth in the central part of the Ryukyu Slab (Figure 3g and Movies S1 and S2), which is connected at its northeastern extent with a major vertical tear (we name the "Jeju Rip") running beneath the immediate southwest of Kyushu and passing beneath Jeju island, South Korea (Figure 5b). Defining the northeastern edge of the Jeju Rip, a thin, steep segment of the slab we refer to as the "Kyushu Tongue" can be traced to 620 km depth along a strong

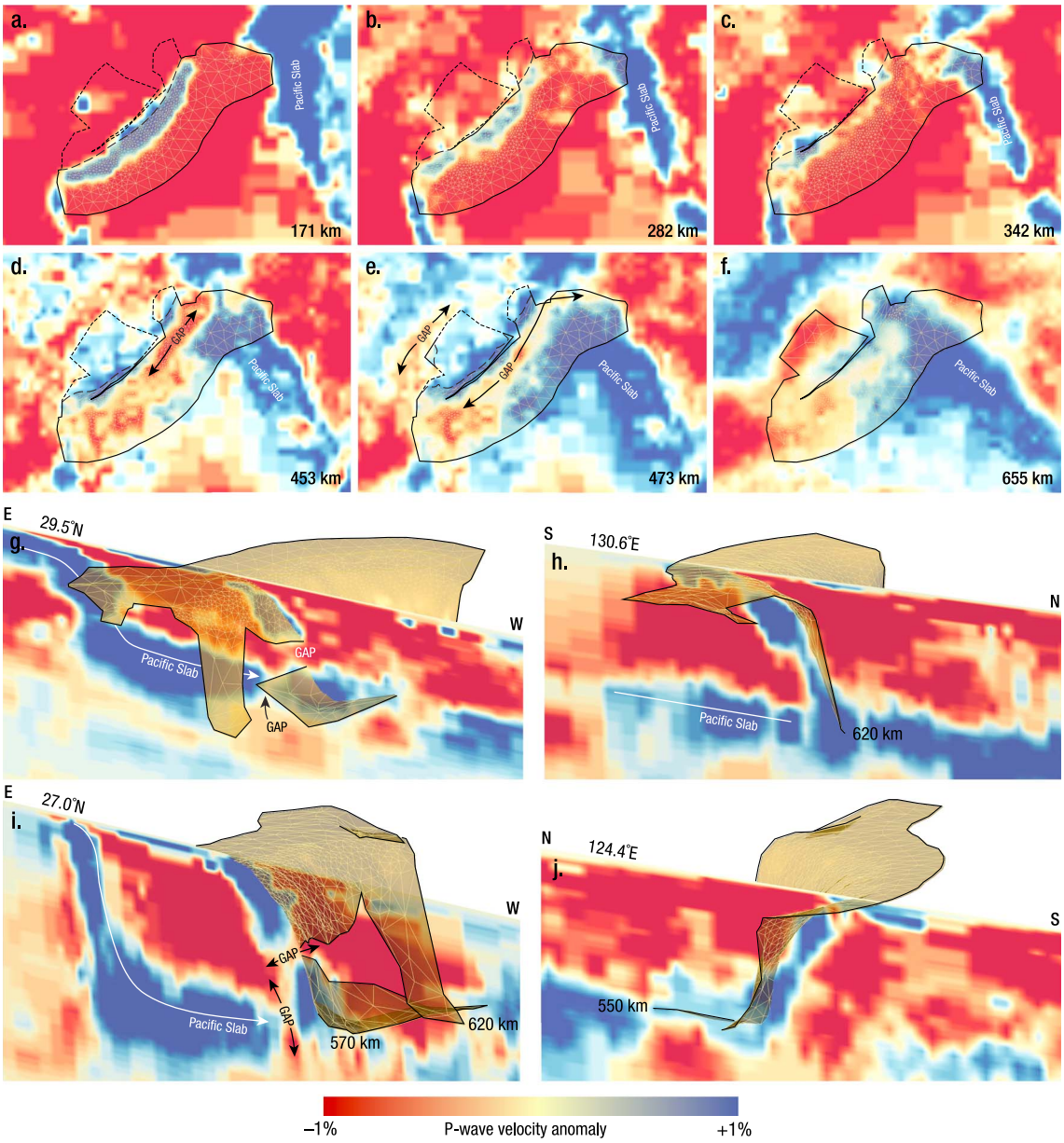

Figure 3. *P* wave tomographic model UU-P07 for the north Philippine region. (a–f) Map views of different depth slices (171, 282, 342, 453, 473, and 655 km depth, respectively) through the data set. Parts of the slab mesh below the plane of section are dotted; the line of intersection is dashed. See also Movie S1 for intervening depth slices, shown with earthquake hypocenter locations from the Engdahl–van der Hilst–Buland (EHB) Bulletin [*Engdahl et al.*, 1998]. (g–j) The Ryukyu and Shikoku slab mesh, compared with vertical cross sections through the *P* wave tomographic model (29.5°N, 130.6°E, 27.0°N, and 124.4°E, respectively). The horizontal tear in the Ryukyu Slab (Figures 3g and 3i) is interpreted from an aseismic zone that correlates with a negative *P* wave velocity anomaly. The slab mesh above this tear is interpreted from seismicity (Figure 2), *not* this tomographic model (following "Rule 2" defined in section 3.3). We interpret there to be a narrow gap between the Pacific Slab (large positive *P* wave anomaly, labeled) and the lower part of the Ryukyu Slab, which both reach a similar depth of 570–620 km. N.b.—for part (i), the view is from below, showing the underside of the slab mesh. See also Movies S2–S4 for additional sets of cross sections, and comparisons with the MIT-P08 *P* wave tomographic model of *Li et al.* [2008] (Movie S3) and SPK_07_1.0 sensitivity test (Movie S4).

positive *P* wave anomaly (Figure 3h and Movie S2 at 137.26° E). We also identified the large slab window (referred to here as the "Shikoku Window") noted also by *Zhao et al.* [2012], *Huang et al.* [2013], *Cao et al.* [2014], and *Lallemand* [2016]—an aseismic region correlating with a slow *P* wave anomaly beneath the island of Shikoku. However, unlike those previous interpretations, and the interpretation of *Wu et al.* [2016], we do not interpret that the Ryukyu Slab rests on top of the Pacific Slab, since a pronounced high negative *P* wave anomaly is shown to separate the lower part of our Ryukyu Slab interpretation from the edge of the fast *P* wave anomaly correlating with the Pacific Slab (Figures 3e and 3i). We therefore interpret that the Kyushu Tongue

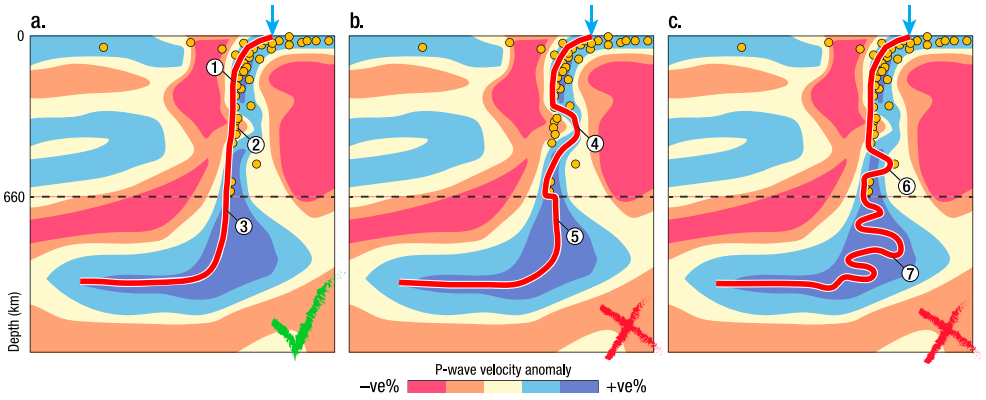

Figure 4. Three different interpretations for the surface of seismicity (red lines) of a fictitious slab. Earthquake hypocenters are shown by the yellow spots, and the trench locations are shown by the blue arrows. (a) Our preferred interpretation, where (1) the upper seismic surface is mapped just above the cluster of hypocenters; (2) the seismicity is favored over the tomography where the two data sets are in conflict; and (3) where the *P* wave tomography is used to extend the slab mesh below 660 km, the trajectory of the slab was maintained by extrapolating along a similar *P* wave anomaly value to that which correlated with the last few hypocenter locations. (b) An interpretation that violates our methodology because (4) the mesh was edited in order to follow the positive *P* wave anomaly in disregard of numerous hypocenters; and (5) the center of the broad positive *P* wave anomaly was chosen arbitrarily, inconsistent with the upper part of the slab, and causing a sharp overhanging step at 660 km depth. (c) Another interpretation that violates our methodology because (6) the mesh deviates to accommodate a single outlying hypocenter; and (7) the mesh is draped back and forth in a totally arbitrary way across the entire extent of the broad positive *P* wave anomaly.

reaches a depth of 620 km, and the part of the Ryukyu Slab beneath the Ryukyu Tear reaches a depth of 570 km (Figure 5b). To clarify our distinction between the Ryukyu and Shikoku slabs, we consider the Jeju Rip to be the boundary.

4. Reverse-Engineering the Effects of Subduction Using *Pplates*

We implemented an approach, developed and first presented by *Lister et al.* [2012], to test the viability of our interpreted slab geometry. This approach seeks to reverse-engineer (*not* forward model) the consequence of subduction by modeling the slab mesh as an elastic sheet. The logic applied is that any geometrically viable slab morphology must have the ability to unfold with minimal area change into a continuous sheet at sea level; conversely, a geometrically implausible slab ought not restore to Earth's surface without considerable internal strain. Analogous to ironing creases from a heavily crumpled shirt, the sequence of events leading to the mesh being unfolded is not important, since all sequences must ultimately yield the same result. Therefore, we sought not to realistically "rewind" subduction but instead to accurately replicate its starting conditions by any transformations necessary.

We performed this simulation using the "Orpheus Engine" built into *Pplates* [*Lister*, 2017a]. Importantly, all calculations were performed using spherical coordinates with zero meters depth modeled as a spherical surface, so as to accurately replicate the geometrical consequences of subducting a lithospheric shell into a spherical Earth [*Lister et al.*, 2012] and to avoid geometric distortions introduced by projections.

4.1. "Floating" the Slab Mesh

Our mesh model was loaded into *Pplates* and reformatted such that it was described entirely by abutting triangular faces. Centroids were then calculated for each face from which straight linkages were made between each centroid and the corners of their respective triangles (Figure 6a). These linkages were assigned fixed spring constants and made to behave perfectly elastically in both extension and compression, outputting strain values as a measure of change in length, which reflects the change in surface area of the triangle. Vectors were attached to each centroid, normal to each face, such that all triangles were assigned consistent polarities. Nodes comprising the oceanic "skirt" were locked in place at their surface locations so that the slab location along the trench would be fixed throughout the slab flotation process (Figure 6b).

External buoyancy forces and horizontal driving forces were then applied to the mesh, encouraging the elastic mesh to unfold and ascend to zero meters depth (Figure 6b and Movies S7 and S8). The applied horizontal

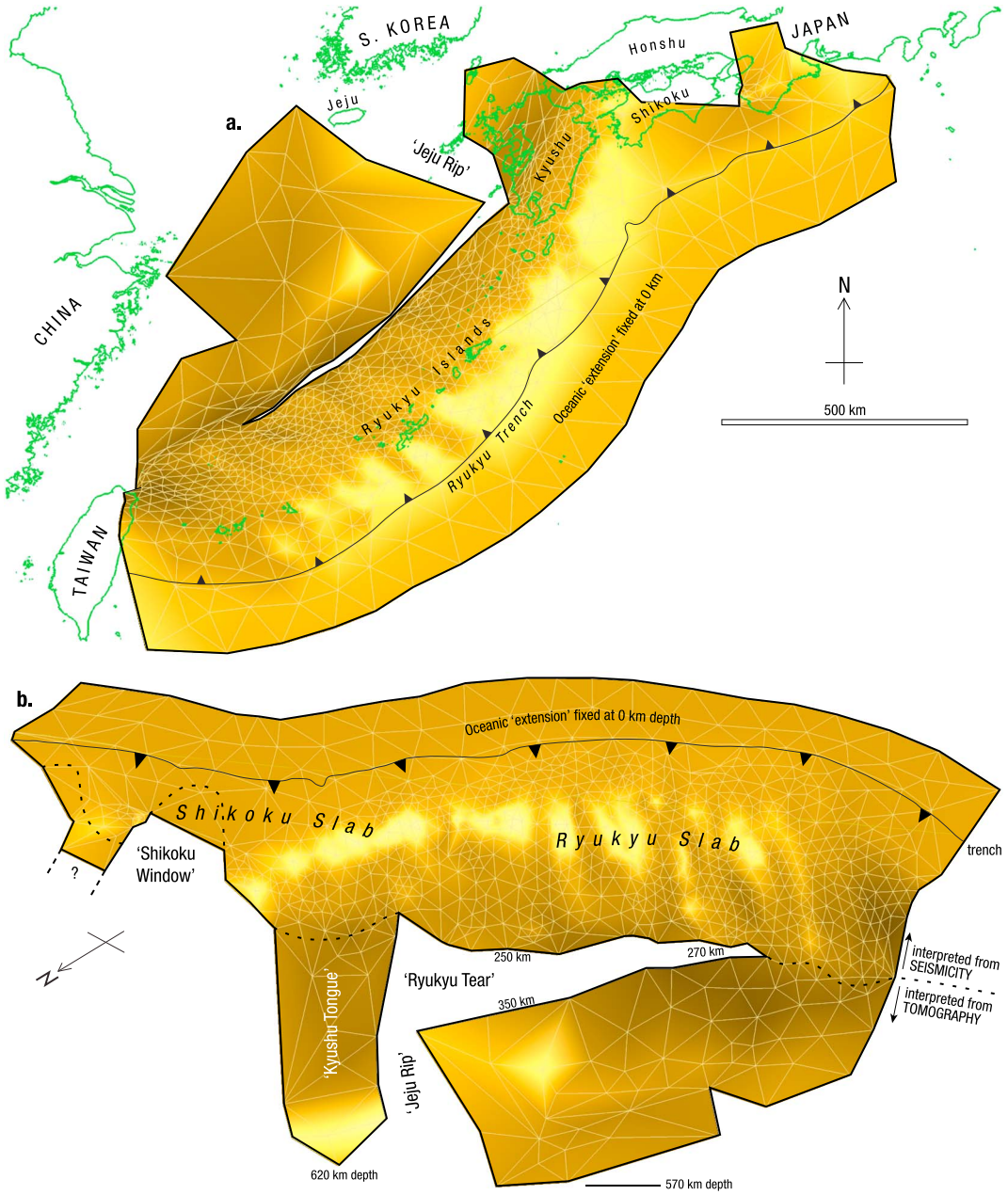

Figure 5. Initial interpretation of the present-day Ryukyu and Shikoku slab geometry, as determined from analysis of hypocenter locations [*International Seismological Centre*, 2016] and *P* wave tomography [*Hall and Spakman*, 2015]. Note the addition of the oceanic "extension" added to the southeast of the Ryukyu Trench. (a) Map view, displaying coastlines in green; (b) view downward from the northwest. Note the decrease in slab mesh density below the level of the inferred slab tear. This is a consequence of the slab's aseismicity below this depth, and the interpretation therefore being based solely on *P* wave tomography below ~270 km. See Figure S2 for a 3-D .pdf of this initial slab model.

forces were applied roughly perpendicular to the trench (Figures 7f–7j), but only because this was the most efficient way to unfold the mesh. These forces are not intended to simulate the effects of reversing plate convergence. As demonstrated in Movie S9, different unfolding pathways ultimately lead to the same configuration, as only one configuration minimizes the internal viscoelastic spring forces in the slab mesh.

Throughout the floating process, the Orpheus Engine effectively simulates a process of viscoelastic adjustment as the mesh seeks to minimize the internal strain of all triangles (Movies S7–S9). As shown in Figure 7, strain is displayed for each face on a red-green-blue scale: green for unstrained, red for negative strain (from compression), and blue for positive strain (from extension). Since the sequence of events causing the mesh to

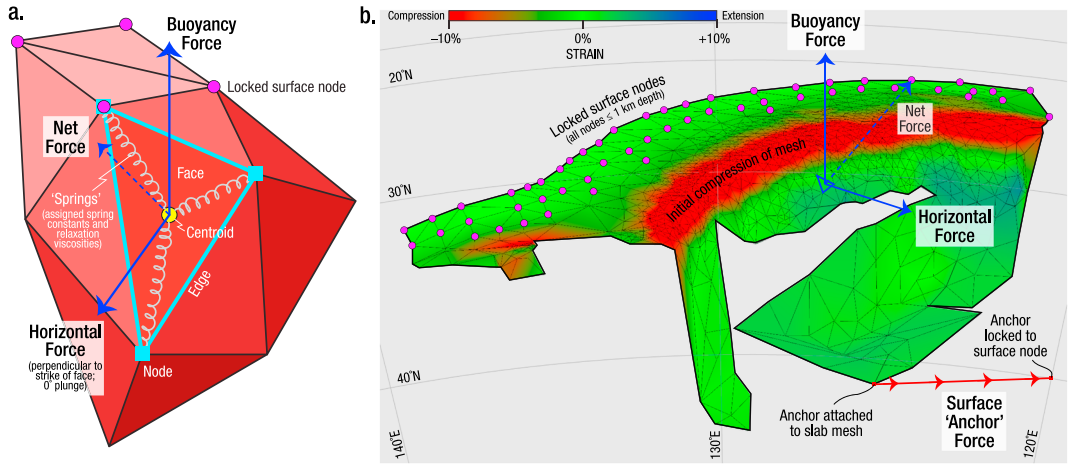

Figure 6. (a) Diagram showing how *Pplates* describes the slab mesh. Nodes are linked by edges that bound triangular faces. Centroids exist in the centee of each triangular face, which are linked by perfectly elastic "spring" forces to the three surrounding nodes. Buoyancy and horizontal forces are applied to each centroid during slab floating. (b) The Ryukyu Slab mesh in the early stages of floating (for an animated version, see Movie S7). Note how the buoyancy and horizontal forces, acting on each centroid in the mesh, cause the mesh to move upward and outward away from the trench (which is held in place by the locked surface nodes, shown here in pink) causing, initially, the top of the mesh to compress (red). Additional "anchor" forces may be applied between any node and any location at the surface. The magnitude of each type of force may be adjusted at any time during the floating operation.

ascend to its presubducted geometry does not matter (because we are *not* attempting to simulate the subduction process), additional forces were applied to the slab (the "Surface Anchor Force" shown in Figure 6b) to tow out corners of the mesh and prevent it from becoming folded during ascent (as occurred, for instance, in Figure 7e). The approach employed here, analogous to shaping pizza dough, was to overstretch the mesh (Figures 7f–7j) and then wait as its internal elastic stresses contract the slab into a state of minimum strain (Figures 7k–7o; see also Movie S8 from 1:01 and Movie S9 from 0:16). Because each face comprising the mesh at all times retains the memory of its own initial geometry and relationship to each of its neighbors and because the linkages behave perfectly elastically and can never "snap," the mesh will always be able to recover from huge distortions and arrive at the same configuration no matter which deformational pathway taken (Movie S9).

Once the mesh had been manipulated by the applied buoyancy and horizontal forces and additional "anchors" (Figures 7f–7j) into a state where all faces were flat, located at 0 km depth, and facing upward (i.e., there were no folds or wrinkles in the mesh), the anchor forces were removed (Figure 7k), and the mesh was left to minimize the residual strain of each face, causing the internal force balance of the mesh to tend toward a state of static equilibrium (Figure 7k–7o).

4.2. Inferring Additional Tears in the Slab Mesh

The next task was to assess to what extent the floated slab (Figure 7o) had validated the original slab interpretation (Figure 5). In other words, how feasible was it for the interpreted slab geometry to have been achieved through the deformation of a rigid lithospheric shell? As illustrated with a generalized example in Figure 8, there are likely to be errors in the initial slab interpretation stemming from the less-than-ideal resolution of the earthquake hypocenter data set and *P* wave tomographic model.

In this generalized example, the shape of the trench is gently S shaped, meaning that the slab features both a concave section and a convex section (Figure 8a). Assuming that ductile deformation of the slab is minimal, both concave and convex sections of the slab may have torn, stretched, or folded in order to have adopted their shape. Mechanically, this deformation is likely accommodated by vertical tears, with the concave section splaying open along one set (of "type-1"), and the convex section closing up along another (of "type-2"). A type-1 tear, since it results in the opening of a gap, may be interpreted from both seismicity patterns (since this gap is likely aseismic) and the *P* wave tomography (since hot asthenosphere that flows through the gap is likely to produce a more negative *P* wave velocity anomaly than the slab). However, since a type-2 tear allows the scissoring together and overlap of two parts of the slab, it will most probably be indeterminable using

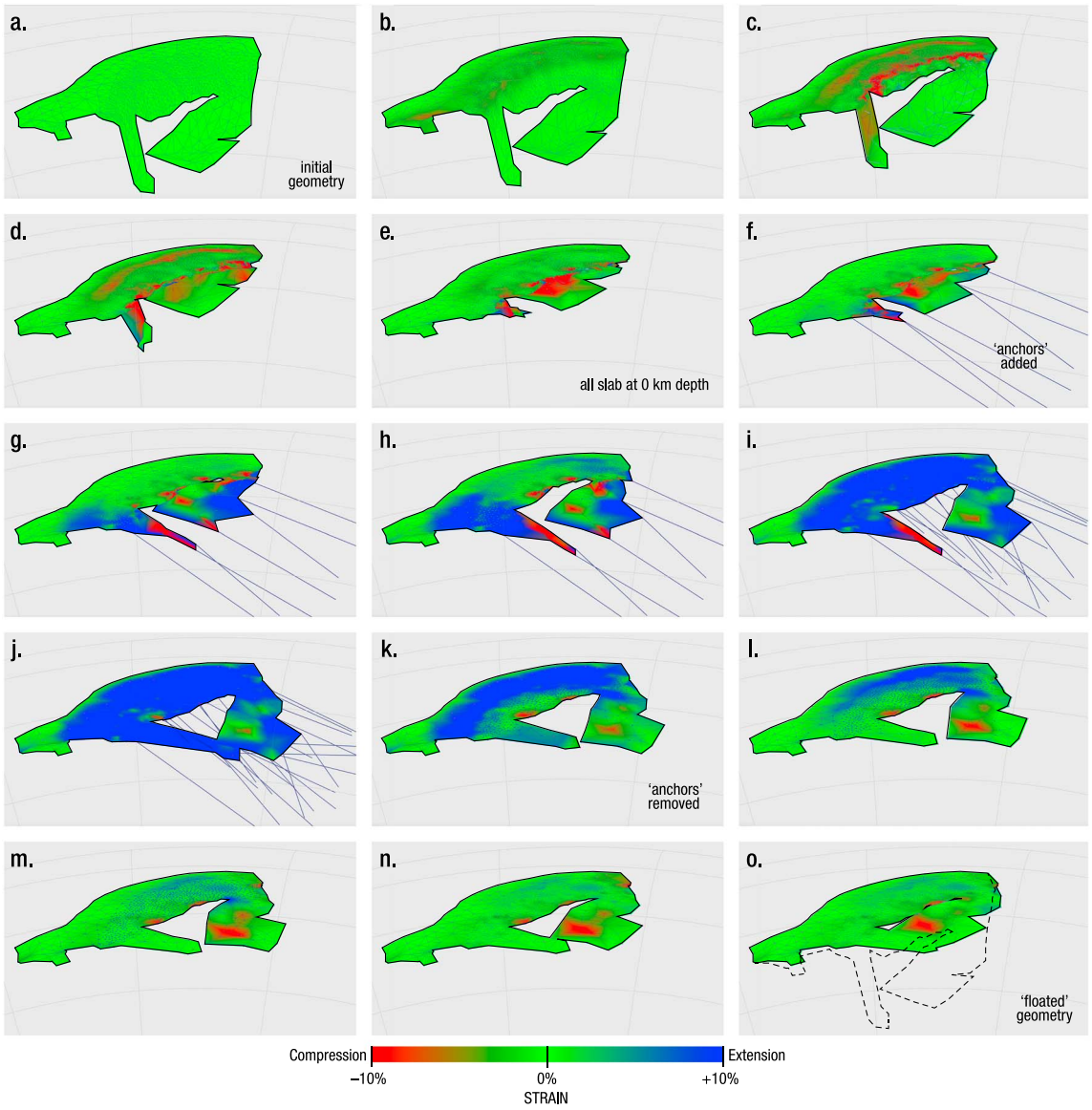

Figure 7. Floating the Ryukyu and Shikoku slabs using the *Pplates* "Orpheus Engine" (see also Movies S7 and S8). (a–e) The slab mesh is "floated" to 0 km depth by the external buoyancy and horizontal forces. (f–j) Anchor forces are applied to pull out creases from the mesh, which cause most of the mesh to be placed into extension. (k–n) The anchor forces are removed, and the mesh contracts elastically as it minimizes its internal strain. (o) The mesh approaches a state of static equilibrium (minimal residual strain). The dashed lines show the initial slab geometry, for comparison. See Figure 9a for a top-down view. Note that in Figure 7e, the mesh was heavily creased, containing many small folds, whereas in Figure 7o, all the creases have been pulled out by the anchors. Note also that locked surface nodes comprising the oceanic "skirt" (displayed as green throughout) successfully fixed in place the southeastern edge of the mesh. Of particular note, the large horizontal tear present in Figure 7a has nearly fully closed in Figure 7o.

these two data sets, especially if the two parts of the slab parallel each other in close proximity (Figure 8b). Furthermore, assuming that type-1 (and/or possibly type-2) tears are identified, their exact sizes may be difficult to ascertain. The slab floating simulation performed by *Pplates* enables this validation procedure, within the limits of the assumptions stated previously.

A floated slab mesh whose triangles underwent no net internal strain after ascent (which, using our color scheme would appear bright green) would demonstrate that the mesh is geometrically plausible, in so far as it can be attained by folding a lithospheric shell. Regions of negative strain (due to compression) would appear red, and regions of positive strain (due to extension) would appear blue (Figure 8c). Due to the arguments outlined in the previous paragraph and in Figures 8a–8c, undetected type-2 tears would result in regions of positive strain, and undetected or under-sized type-1 tears would result in regions of negative strain in the floated mesh. Therefore, the sign (+ or –) of the strain is diagnostic of the type of tear that has been

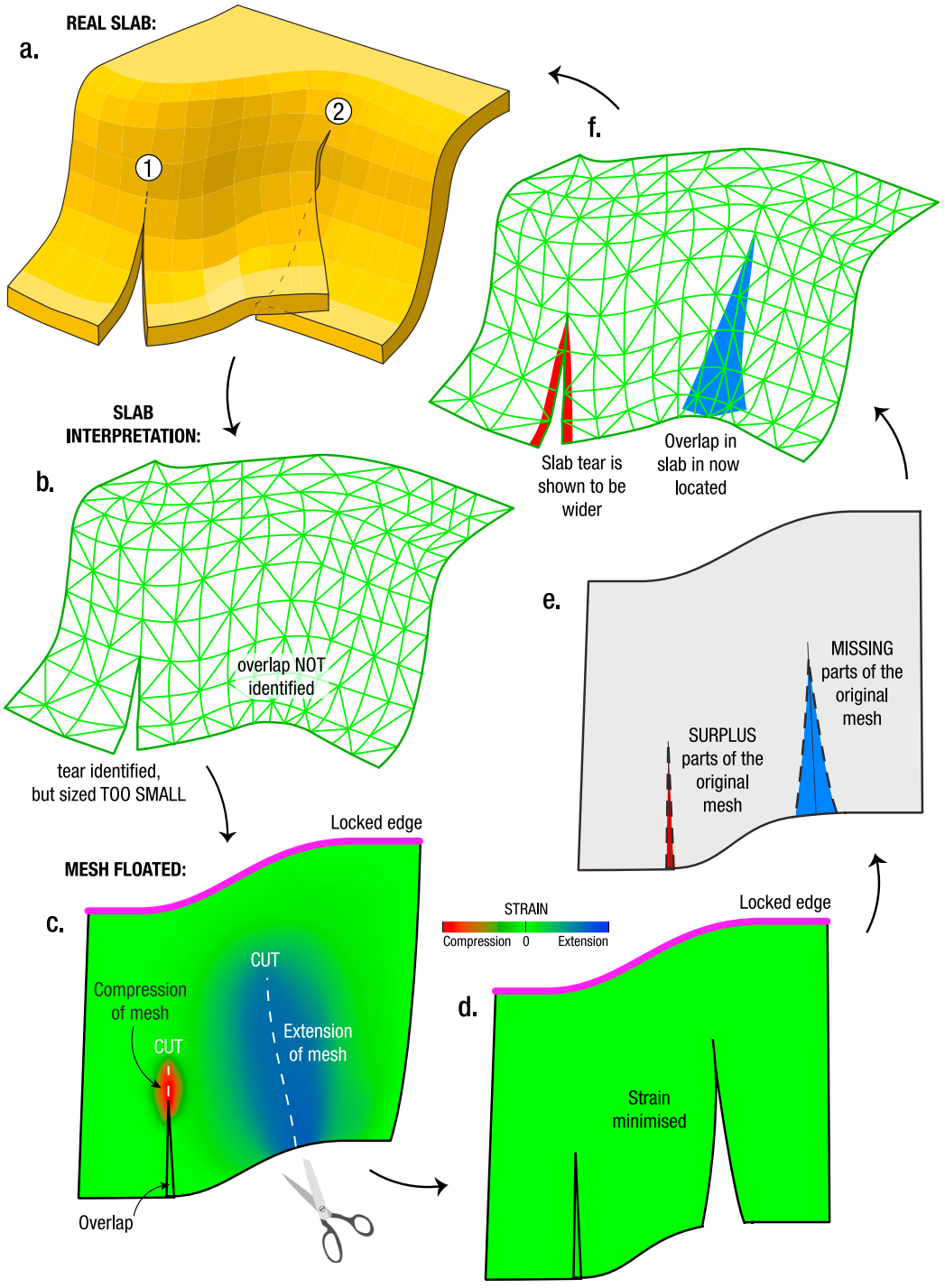

Figure 8. Methodology for reverse-engineering subducted slabs. (a) The actual slab geometry sought to be modeled (a fictitious example), featuring two tears: "type-1" and "type-2." (b) The initial slab mesh, interpreted using seismicity and tomographic models. These two data sets are, as depicted here, likely insufficient to resolve the overlapping part of the slab along the type-2 tear. Small tears may also be unresolved, and the true extent of larger tears, such as the type-1 tear, may not be fully realized. (c) The process of floating the slab using *Pplates* demonstrates that this initial interpretation is geometrically implausible, because the mesh can only be unfolded if it undergoes considerable internal strain. These strained regions indicate where extra tears are required, as shown by the white dotted lines. (d) After these tears are introduced, *Pplates* is able to relax the mesh to achieve minimal residual strain, thereby validating the tear locations. (e, f) Overlaps that occur within the floated mesh relate to overestimations of slab size in the original model; and gaps that occur within the floated mesh relate to an initial underestimation of slab size, in this instance the overlap along the type-2 tear.

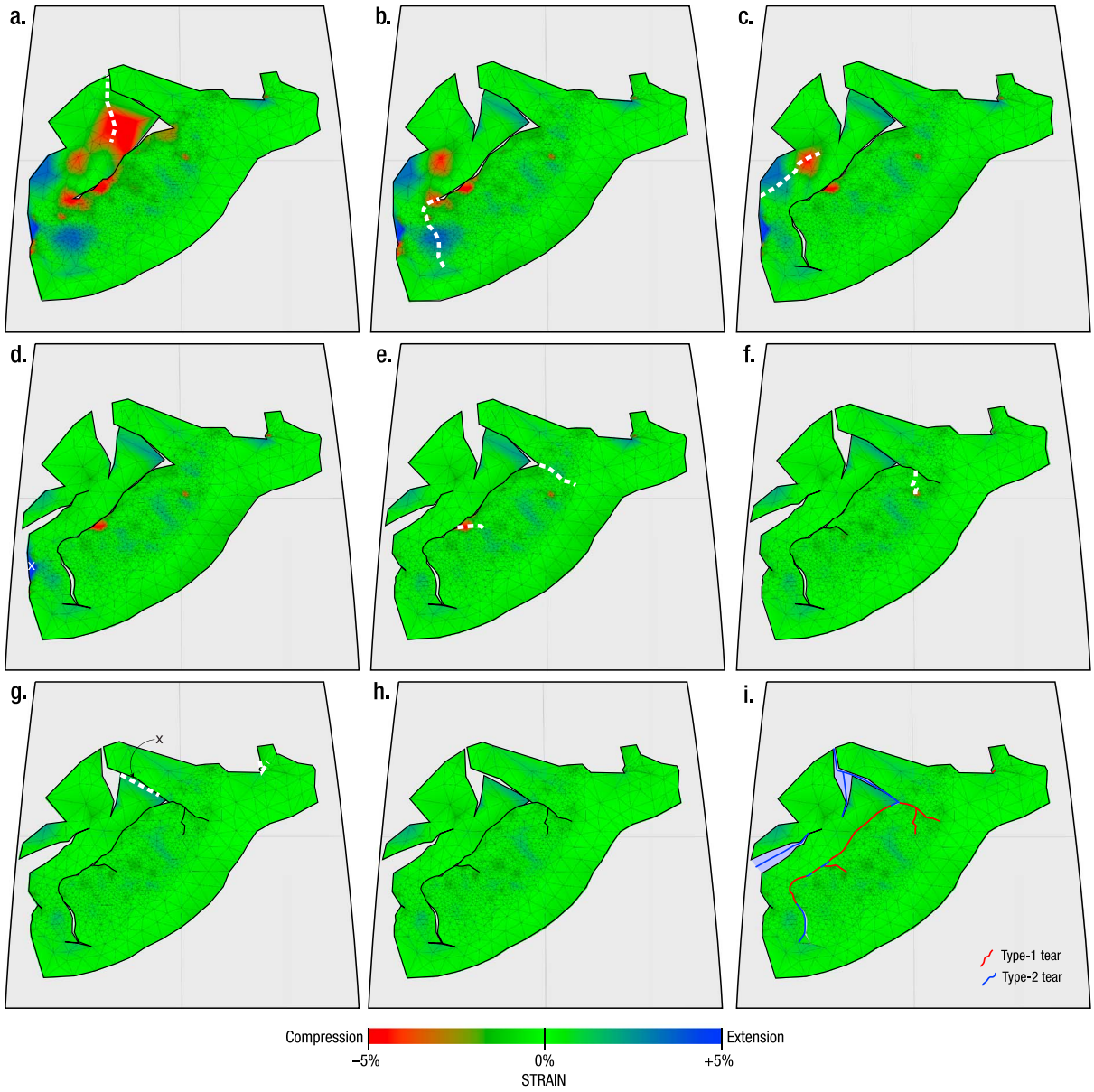

Figure 9. Determining the locations of necessary tears in the Ryukyu Slab using *Pplates*. Note the change of scale since Figure 7—red and blue now represent −5% and +5% strain, respectively. (a) The original slab model, floated to the surface before any additional cuts being made. (b–h) The results of introducing incrementally more cuts to the slab mesh, as shown by the white dotted line in the previous part of the figure. In Figures 9d and 9g, faces have been deleted (indicated by the crosses). (i) The "final" floated mesh, with residual strain lowered beneath 1% across the whole slab, overlain with the locations of all tears (red lines—type-1 tears; blue lines—type-2 tears). Each map shows an area between 120–140°E and 20–40°N. See Figure S3 for an alternative version of Figure 9i where strain values are colored between −1% and +1%. A "background" of short-wavelength positive and negative strain fringes of <1% (Figure S3) is an unavoidable consequence of forcing one curved surface to adopt the curvature of another and demonstrates the necessity for small amounts of ductile deformation in addition to slab tears.

overlooked in the original interpretation, and the locations and orientations of those strained regions are indicative of where the tears should be located. As shown for the generalized example in Figures 8c and 8d, the introduction of tears through the strained regions leads to the removal of residual strain in the mesh by allowing the free edges to move, and triangles bound within to reconfigure toward a static equilibrium of zero (or minimal) strain as the stresses of the spring forces dissipate.

4.3. Application to the Ryukyu and Shikoku Slabs

In the real example of our Ryukyu and Shikoku slab mesh, as shown in Figures 7o and 9a, the mesh could be floated to 0 km depth only if some regions underwent up to ±5% strain. This demonstrates the necessity

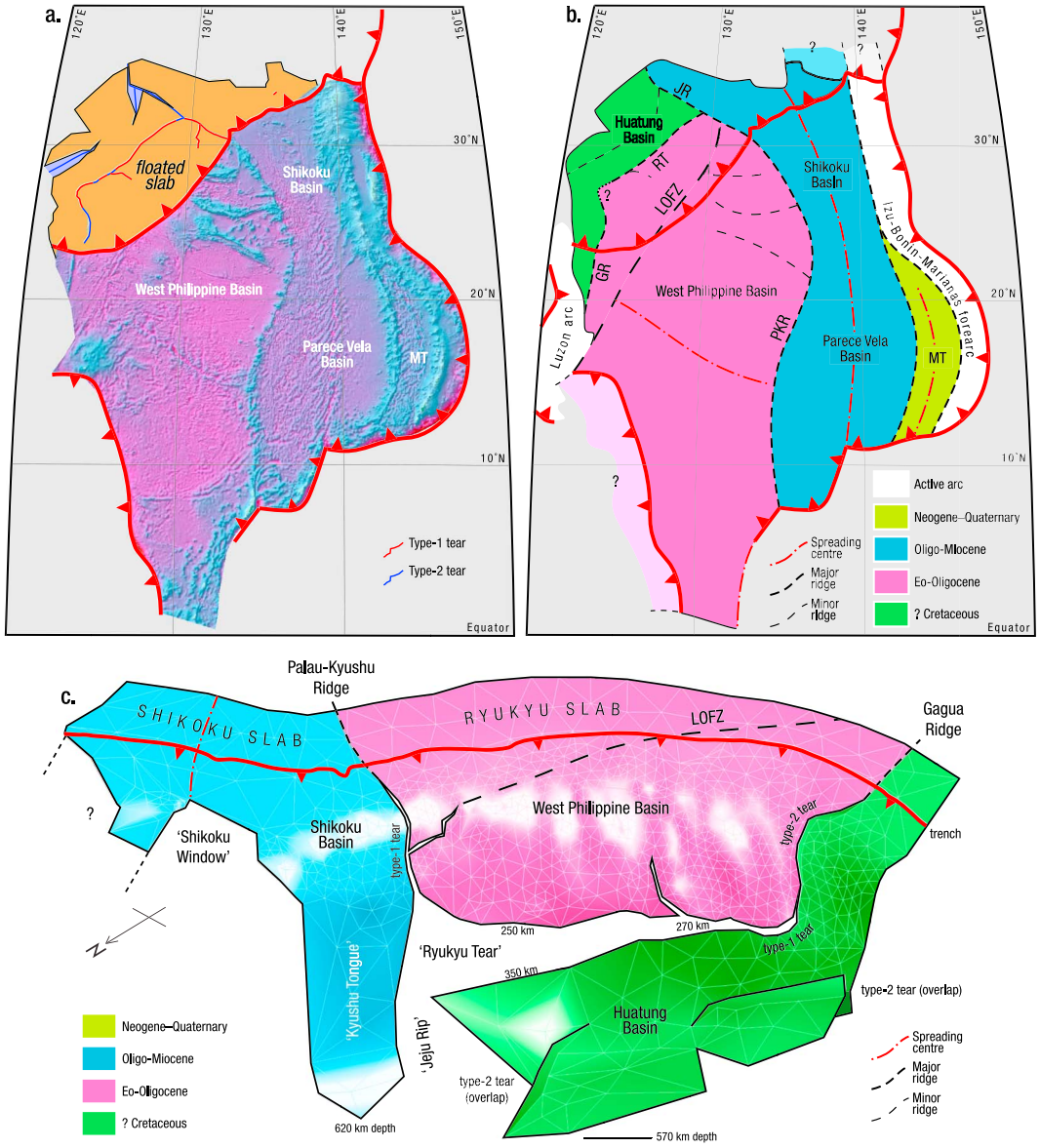

Figure 10. Final interpretation of the Ryukyu and Shikoku slabs. (a) The "floated" slab mesh (taken from Figure 9i) connected at the Ryukyu Trench to the Philippine Sea Plate. (b) Interpretation of the configuration of the Philippine Sea Plate, prior to subduction of its northern margin. (c) Reverse-engineered slab model (which is to Figure 8f as Figure 5b is to Figure 8b) showing how the slab ripped open along the subducted Palau-Kyushu and Gagua ridges, and the boundary between the Huatung and West Philippine Basin. Basin ages taken from *Lallemand* [2016]. PKR—Palau-Kyushu Ridge; GR—Gagua Ridge; LOFZ—Luzon-Okinawa Fracture Zone; RT—(proto) Ryukyu Tear; JR—Jeju Rip; and MT—Mariana Trough.

for tears through these regions. Figure 9 documents the series of cuts to the slab mesh that were required to reduce its residual strain to minimal levels. (By "minimal levels," we refer to values <1%.)

First of all, the floated slab is shown to validate the first-order geometric features of the original model, specifically the wide, wedge-shaped horizontal Ryukyu Tear running through the slab. As shown in Figures 7j–7o and 9a, the upper and lower edge of this wide gap neatly closed during the floating process. Also, the northwestern limit of this lower section rose to match very closely with the edge of the narrow, elongate Kyushu Tongue segment of the slab, along the Jeju Rip.

However, several second-order features of the slab were revealed to have geometric infeasibilities. The lower section of the Ryukyu Slab, which was interpreted purely from *P* wave tomography (and so interpreted with

higher uncertainty), was subject to significant compressional strain (−5%). This is unsurprising, given the original interpretation featured a concave "spoon"-type feature (seen best in Figures 3g and 3i) that clearly cannot be flattened without compression in the center (or extension around the rim). This feature was restored by introducing a short N-S tear into the strained region (Figures 9a and 9b). The next largest anomaly, a region of positive strain in the southwest of the slab, was restored by extending the major horizontal tear, via a 90° kink, to a trench-perpendicular tear (Figures 9b and 9c). A shorter tear was then introduced to the western part of the floated slab to restore the regions of positive and negative strain shown in Figure 9c. Apart from minor cuts being made, the last modifications were to extend the tear in the slab between the Shikoku and Ryukyu segments in a direction subparallel to the trench (Figures 9e and 9f) and to trim the extent of the lower part of the slab along the same trajectory (Figures 9g and 9h).

It is important to note that several different configurations of additional tears were trialed that were unsuccessful in effectively minimizing the residual strain before the solution presented here in Figure 9 was discovered.

4.4. Presenting the Most Plausible Slab Morphology

The final floated mesh interpretation is shown in Figure 10a, annotated with the locations of all tears (type-1 tears in red; type-2 tears in blue). Following the logic outlined in Figure 8, we trimmed overlapping parts of the mesh either side of type-1 tears and extended the mesh across the gaps either side of type-2 tears, to present our final slab interpretation in Figures 10b and 10c.

5. Discussion

5.1. Previous Interpretations of Slab Seismicity and Tomography

Lallemand et al. [2001], based on the *P* wave tomographic model of *Bijwaard et al.* [1998], interpreted an asymmetry in the (largely aseismic) Ryukyu Slab, noting that it can be traced down to 670 km depth west of the Gagua Ridge by Taiwan (shown also by *Gutscher et al.* [2016]), but that toward the east, it could be traced to only ~250 km depth before encountering a wide low-velocity zone. A second, deeper, high-velocity zone existing farther beneath this (at ~500–660 km depth) was interpreted by *Lallemand et al.* [2001] to belong primarily to the underlying Pacific slab, but also to detached parts of the Philippine Sea Plate; thus, the authors inferred the presence of a large horizontal gap. Furthermore, they hypothesized that this horizontal gap may connect to the southwest with the subducted part of the Gagua Ridge, suggesting that the West Philippine Basin and Huatung Basin lithosphere would have detached from each other as they were subducted [*Lallemand*, 2016]. *Wei et al.* [2015] also noted a peculiarity with the westernmost part of the slab, since their *S* wave (but not *P* wave) tomogram showed that a slab-like high-velocity zone penetrates the 660 km mantle discontinuity in the region west of the Gagua Ridge. *Zhao et al.* [2012] further interpreted, using high-resolution *P* wave tomography, that the Shikoku portion of the Philippine Sea plate reaches as deep as 430 km beneath Kyushu and 370 km under Honshu (western Japan).

Various authors have suggested that upon subduction, the Philippine Sea Plate broke apart along the subducted Kyushu-Palau Ridge, separating into the Ryukyu (southwestern) and Shikoku (northeastern) slab segments [*Huang et al.*, 2013; *Cao et al.*, 2014; *Wu et al.*, 2016; *Lallemand*, 2016]. *Huang et al.* [2013] further noted that hot mantle upwelling, generated due to deep dehydration of the underlying "stagnant" Pacific Slab [*Zhao et al.*, 2012], may have contributed to the thermal anomaly and enlargement of the slab window. However, *Lallemand* [2016] noted that the location of this interpreted window is misaligned with the trajectory of the Kyushu-Palau Ridge south of the trench and suggested that this is most likely reconciled by 150–200 km of right-lateral offset along the Luzon-Okinawa Fracture Zone. *Wu et al.* [2016] made the alternative interpretation that this slab window is unrelated to the Kyushu-Palau Ridge and instead produced by detachment of their "West Shikoku" slab downdip of the Shikoku Basin fossil spreading ridge. These authors instead proposed that the trace of the subducted Kyushu-Palau Ridge correlates with a sharp dropoff in seismicity along a trajectory requiring no offset along the Luzon-Okinawa Fracture Zone.

5.2. Tectonic Implications of the "Reverse-Engineered" Slabs

The process of reverse-engineering the Ryukyu and Shikoku slabs has revealed that major tears (or, alternatively, discrete zones of localized ductile shear) must have accommodated their deformation during subduction (Figure 10). Importantly, the locations of these tears align closely to ridges, spreading centers, and fracture zones present in the unsubducted part of the ocean; thus, it is possible, by extrapolating these features, to produce a reconstruction the subducted northern margin of the Philippine Sea plate (Figure 10b).

First of all, we interpret that the Palau-Kyushu Ridge, upon subduction at the junction of the Ryukyu Trench and Nankai Trough, broke open to form the Jeju Rip. Second, the floating process suggests the existence of a tear in the western Ryukyu Slab (Figures 9b and 9c) that aligns with the Gagua Ridge, and we therefore interpret that the Gagua Ridge must also have torn open as it was subducted. Third, tears resulting from subduction of the Palau-Kyushu and Gagua ridges are connected by a subhorizontal; trench-parallel tear in the Ryukyu Slab (the Ryukyu Tear; Figure 10c) that we interpret was formed by unzipping the contact between the West Philippine and Huatung basins. Fourth, subduction of the fossil spreading center that opened the Shikoku Basin aligns with the Shikoku Window in the center of the Shikoku Slab. And fifth, the subducted Luzon-Okinawa Fracture Zone aligns with, and so *may* have created, a minor tear in the Ryukyu Slab that intersects the Jeju Rip (flagged in Figure 9f). The T junction created by the intersection of the Ryukyu Tear with the Jeju Rip confirms that the Shikoku Basin must be younger than the West Philippine Basin and Huatung Basin.

Our interpretation differs in a few ways to previous proposals. Whereas we interpret that the Ryukyu Slab reaches as deep as 570 km and the Kyukyu Tongue of the Shikoku Slab as deep as 620 km (Figure 10c), previous authors have interpreted deep and slow *P* wave anomalies to instead relate to the Pacific slab [e.g., *Wu et al.*, 2016], using the MITP08 *P* wave tomographic model of *Li et al.* [2008]. However, we argue that the UU-P07 *P* wave tomographic model of *Amaru* [2007] shows prominent linear high-velocity zones that separate the Ryukyu and Shikoku slabs from the Pacific slab at ~ 450–600 km depth (Figures 3d, 3e, 3g, and 3i). The anomalies underpinning this interpretation are demonstrated by the sensitivity testing of the UU-P07 *P* wave model to be sufficiently resolved spatially (Movies S4–S6).

Furthermore, while we interpret that the subducted Palau-Kyushu Ridge broke open as the Jeju Rip, most other authors interpreted that it instead formed the Shikoku Window before it was somehow offset [*Lallemand et al.*, 2001; *Huang et al.*, 2013; *Cao et al.*, 2014; *Lallemand*, 2016]. The significant misalignment of the Palau-Kyushu Ridge with the Shikoku Window was noted by *Lallemand* [2016], who accounted for it by invoking 150–200 km of right-lateral offset along the Luzon-Okinawa Fracture Zone. However, the slab model validated by our reverse-engineering methodology does not require the Luzon-Okinawa Fracture Zone to have caused such large displacements. We agree with the interpretation of *Wu et al.* [2016] that formation of the Shikoku Window can be attributed to subduction of the fossil spreading center of the Shikoku Basin, and that subduction of the Palau-Kyushu Ridge produced a separate tear. However, *Wu et al.* [2016] did not identify the Jeju Rip (or Ryukyu Tear), and as such the extrapolation of their tear follows a different (less eastbound) trajectory.

Although we attribute subduction of the fossil spreading center, not the Palau-Kyushu Ridge, to formation of the Shikoku Window, it is of course still a valid interpretation that volcanism and mineralization in southwest Japan has been systematically influenced by the shifting location of this gap [*Watanabe*, 2005; *Nakajima and Hasegawa*, 2007; *Mahony et al.*, 2011; *Cao et al.*, 2014; *Pi et al.*, 2016]. Our slab model (Figure 10c) would further suggest that volcanism on Jeju Island (Figure 5a), located above the Jeju Rip, may be influenced by fluids and magmas funneling through this gap between the sinking, rolling back slabs [cf. *Brenna et al.*, 2015].

Our "floated" slab configuration shown in Figure 10b has several key similarities to that presented by *Lallemand* [2016], in that the Huatung Basin originally comprised the northwestern edge of the Philippine Sea Plate, connected to the West Philippine Basin by the Gagua Ridge and a trench-parallel boundary at depth [*Lallemand et al.*, 2001]. Our work supports the conclusions of *Lallemand et al.* [2001], *Lin et al.* [2004, 2013], and *Lallemand* [2016] that the contacts between these juxtaposed pieces of oceanic lithosphere broke open as the slab descended. Also, both the reconstruction we present in Figure 10b and that by *Lallemand* [2016] feature a tight kink where the subducted Gagua Ridge meets the (proto-)Ryukyu Tear. *Mrozowski et al.* [1982], *Hilde and Lee* [1984], and *Deschamps et al.* [1998] interpreted the Gagua Ridge as a former fracture zone, in which case the kink in the Huatung Basin-West Philippine Basin contact most likely represents the southwestern limit of a rift terminated by this former "Gagua Fracture Zone" (or oceanic transform). This implies that the Huatung Basin oceanic lithosphere must have also bounded the south of the West Philippine Basin before it rifted open. A further implication is that the Huatung Basin must be older than the oldest part of the West Philippine Basin—so older than 54 Ma [*Deschamps and Lallemand*, 2002]—in conflict with those studies proposing a much younger age for the Huatung Basin lithosphere [*Sibuet et al.*, 2002; *Kuo et al.*, 2009; *Doo et al.*, 2015; *Gutscher et al.*, 2016]. Hence, as suggested by *Deschamps et al.* [2000] and *Lallemand et al.* [2013],

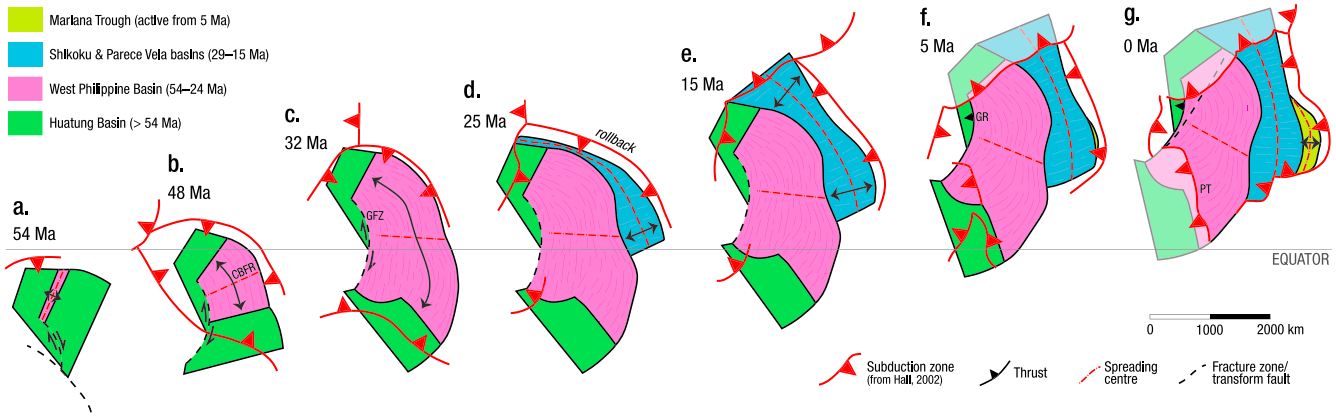

Figure 11. Schematic tectonic reconstructions depicting the evolution of the Philippine Sea Plate since 54 Ma. Palaeolatitudes, plate rotations, and the locations of subduction zones follow *Hall* [2002]. Subducted lithosphere (lighter shading) is depicted "floated" to the surface, just like in Figure 10b. (a–c) Rifting of oceanic lithosphere comprising the Huatung Basin (which in this scenario must be >54 Ma) to open the West Philippine Basin from 54 Ma [*Deschamps and Lallemand*, 2002] is accommodated along its western extent by the Gagua Fracture Zone (GFZ), following the interpretation of *Hilde and Lee* [1984]. (d, e) Rollback of the Izu-Bonin arc opened the (southern) Parece Vela Basin from 29 Ma [*Okino et al.*, 1998], and the (northern) Shikoku Basin from 25 Ma [*Okino et al.*, 1994]. (f, g) Subduction of the northern margin of the West Philippine Basin, Huatung Basin, and Shikoku Basin matured from 15 Ma [*Mahony et al.*, 2011] shortly after the Shikoku basin stopped rifting [*Sibuet et al.*, 2002; *Sdrolias et al.*, 2004]. The GFZ is shown to have reactivated as a thrust [*Eakin et al.*, 2015], forming the Gagua Ridge (GR). We propose that at this time, the southern segment of the Huatung basin, and the fringes of the southern West Philippine Basin, began to subduct along the Philippine Trench (PT). (If spreading was symmetrical either side of the Central Basin Fault rift, then the Huatung Basin-West Philippine Basin contact would have descended ~200 km down the Philippine Trench, and the southern part of the Huatung Basin, if still attached, would be totally consumed.) From 5 Ma [*Yamazaki et al.*, 2003], rollback of the Mariana slab rifted open the Mariana Trough. Figure 11g should be compared directly with Figures 10b and 10c.

AGU Tectonics
10.1002/2017TC004686

the Huatung Basin could be Cretaceous, and the 123–105 Ma $^{40}Ar/^{39}Ar$ amphibole ages for dredged gabbros dated by *Deschamps et al.* [2000] may relate to the age of the Huatung Basin. To conclude, we interpret that the Ryukyu Tear most likely propagated along the rifted margin of the Huatung Basin against where spreading of the West Philippine Basin initiated at 54 Ma.

5.2.1. Reconstructing the Philippine Sea Plate

We illustrate our interpretation for the formation of the Huatung and West Philippine basins in a schematic tectonic reconstruction presented in Figure 11. Taking paleolatitudes, plate rotations, and the locations of subduction zones from *Hall* [2002], we depict how the development of a new spreading center in the Huatung Basin, to open the West Philippine Basin from 54 Ma, might have been accommodated along one side by the Gagua Fracture Zone ("GFZ" in Figure 11c), prior to its reactivation as a thrust (Figure 11f). As also depicted, this extension (plus rotation) would likely have been driven by northward rollback of the Pacific Slab and by southward rollback of the east Philippines arc from 54 to 32 Ma [*Hall*, 2002].

Assuming that spreading was symmetrical about Central Basin Fault Rift (discounting complexities noted by *Hilde and Lee* [1984]), the southern part of the Huatung Basin lithosphere would have been entirely consumed along the Philippine Trench, and the West Philippine Basin-Huatung Basin contact (if still connected) would occur at ~ 200 km depth down the Philippine Slab. Figure 11g shows how the current-day basin configuration, inferred from our reverse-engineering of the Ryukyu and Shikoku slabs, could have been achieved by this Huatung Basin rifting scenario.

5.3. Implications and Limitations of Reverse-Engineering

The slab model for the Ryukyu and Shikoku slabs presented in Figure 10c is demonstrated by the reverse-engineering approach to be geometrically viable, insofar as it may be attained by deforming a single oceanic shell. The first-order features within the slab—the Ryukyu Tear and Jeju Rip—have been resolved sufficiently by the UU-P07 *P* wave tomography (Movies S4–6) and are demonstrated by the slab floating process to have been fundamental in controlling slab deformation during subduction. It is important also to emphasize that the alignment of these features with the nonsubducted sections of the Gagua Ridge and Palau-Kyukyu Ridge was indicated entirely by the residual strain distribution of the initial floated mesh (Figure 9a). These subducted ridges almost certainly tore open (as opposed to becoming boudinaged) due to their broad width, their aseismicity, and the magnitude of corresponding negative *P* wave anomalies. This result demonstrates how preexisting oceanic structures may influence the geodynamics of subduction.

Smaller-scale defects such as those in the deep part of the Huatung Basin section may also be tear or alternatively may be zones of ductile shear. But it must also be stressed that the resolution of the *P* wave tomography for these sub-50 km-scale features is likely insufficient to precisely define their intricacies. For both reasons, caution needs to be taken when accepting the results of this reverse-engineering approach for small-scale features.

It is our intention that this reverse-engineering methodology is applied to many further examples, in order to reconstruct the geometries of subducted oceanic lithosphere and to locate structures that later developed into tears.

6. Summary of "Reverse-Engineering" Method

1. A three-dimensional slab mesh was constructed based on earthquake hypocenter distributions and the *P* wave tomography model UU-P07.
2. Using the "Orpheus Engine" of *Pplates* [*Lister*, 2017a], this mesh was made to behave as a viscoelastic sheet. Forces were then applied to ascend the mesh to the Earth's (spherical) surface. This "slab floating" process did *not* attempt to model subduction but rather test the geometric viability of the slab model.
3. After floating the mesh to 0 km depth, faces comprising the slab mesh were left to undergo viscous relaxation, causing the mesh to internally deform toward a state of static equilibrium. The net strain of each face was displayed graphically.
4. The residual strain of each part of the mesh demonstrated where tears were necessary for the slab to have adopted its current morphology. The sign of the residual strain was a useful indicator of the presence of "type-1" (causing a gap) or "type-2" (causing an overlap) tears.
5. Based on this information, cuts were made incrementally to the mesh to minimize its residual strain (this procedure required several different cut configurations to be tested before the optimal solution was found).

6. The locations of these additional cuts were used to infer where tears were required in the original slab model. The floated slab model, plus the additional tears, then served as a "reverse-engineered" reconstruction of the subducted oceanic lithosphere.

7. Conclusions From "Reverse-Engineering" the North Philippine Sea Plate

1. The Ryukyu Slab was subducted to 570 km depth, and the Shikoku Slab to 620 km depth (at the tip of a narrow part of the slab we name the "Kyushu Tongue").
2. Subduction of the Palau-Kyushu Ridge ripped open as a vertical slab tear, the "Jeju Rip," which is currently located beneath Jeju Island. This tear defines the boundary between the Ryukyu Slab and the Kyushu Tounge of the Shikoku slab.
3. Subduction of the Gagua Ridge ripped open as another vertical slab tear, which connects via a 90° bend to a trench-parallel tear we name the "Ryukyu Tear" at 270 km depth. The Ryukyu Tear is terminated by the Jeju Rip to the northeast.
4. Subduction of the fossil spreading center of the Shikoku Basin led to the formation of the "Shikoku Window" beneath eastern Shikoku Island.
5. No major offset along the Luzon-Okinawa Fracture Zone is necessary to account for the locations of the slab tears with respect to Philippine Sea ridges. This fracture zone likely terminates against the Jeju Rip.
6. Since the Gagua Ridge is a former fracture zone, the Ryukyu Tear most likely represents the rifted margin of the Huatung Basin along which spreading of the West Philippine Basin initiated at 54 Ma (Figure 11a). The Huatung Basin must therefore be older than 54 Ma, and possibly Cretaceous.
7. The implication of our scenario involving the Huatung Basin rifting to form the West Philippine Basin (assuming that spreading was symmetrical about the Central Basin Fault Rift) is that the southern half of the Huatung Basin lithosphere would have been fully consumed along the Philippine Trench, if still attached.

Acknowledgments
We would like to thank reviewers Serge Lallemand and Vlad Manea, and Editors Mihai Ducea and John Geissman, for their comments and support. The data used to inform the conclusions of this paper are listed in the references and included as supporting information (Movies S1–S6). This research was funded by Australian Research Council (ARC) DECRA fellowship DE160100128 (awarded to Pownall), ARC grants DP120103554 and LP130100134, and also supported by the Research Council of Norway (Norges Forskningsråd) through its Centres of Excellence funding scheme, project 223272.

References

Amaru, M. L. (2007), *Global Travel Time Tomography with 3-D Reference Models*, Utrecht Univ., Utrecht, Netherlands.
Ansell, J., and D. Adams (1986), Unfolding the Wadati-Benioff zone in the Kermadec-New Zealand region, *Phys. Earth Planet. Inter.*, *44*(3), 274–280.
Aoki, I., and E. Takahashi (2004), Density of MORB eclogite in the upper mantle, *Phys. Earth Planet. Inter.*, *143*, 129–143.
Bijwaard, H., W. Spakman, and E. R. Engdahl (1998), Closing the gap between regional and global travel time tomography, *J. Geophys. Res.*, *103*(B12), 30,055–30,078.
Brenna, M., S. J. Cronin, G. Kereszturi, Y. K. Sohn, I. E. M. Smith, and J. Wijbrans (2015), Intraplate volcanism influenced by distal subduction tectonics at Jeju Island, Republic of Korea, *Bull. Volcanol.*, *77*(7), 16.
Cao, L., Z. Wang, S. Wu, and X. Gao (2014), A new model of slab tear of the subducting Philippine Sea Plate associated with Kyushu-Palau Ridge subduction, *Tectonophysics*, *636*, 158–169.
Chatelain, J. L., B. Guillier, and J. P. Gratier (1993), Unfolding the subducting plate in the central New Hebrides island arc: Geometrical argument for detachment of part of the downgoing slab, *Geophys. Res. Lett.*, *20*(8), 655–658.
Chertova, M. V., W. Spakman, A. P. van den Berg, and D. J. J. van Hinsbergen (2014), Absolute plate motions and regional subduction evolution, *Geochem. Geophys. Geosyst.*, *15*(10), 3780–3792, doi:10.1002/2014GC005494.
Chou, H.-C., B.-Y. Kuo, S.-H. Hung, L.-Y. Chiao, D. Zhao, and Y.-M. Wu (2006), The Taiwan-Ryukyu subduction-collision complex: Folding of a viscoelastic slab and the double seismic zone, *J. Geophys. Res.*, *111*, B04410, doi:10.1029/2005JB003822.
Davies, J. H. (1999), The role of hydraulic fractures and intermediate-depth earthquakes in generating subduction-zone magmatism, *Nature*, *398*(6723), 142–145.
DeMets, C., R. G. Gordon, and D. F. Argus (2010), Geologically current plate motions, *Geophys. J. Int.*, *181*(1), 1–80.
Deschamps, A., and S. Lallemand (2002), The West Philippine Basin: A Paleocene-Oligocene backarc basin opened between two opposed subduction zones, *J. Geophys. Res.*, *107*(12), 2322, doi:10.1029/2001JB001706.
Deschamps, A., P. Monie, S. Lallemand, S. K. Hsu, and K. Y. Yeh (2000), Evidence for Early Cretaceous oceanic crust trapped in the Philippine Sea Plate, *Earth Planet. Sci. Lett.*, *179*(3–4), 503–516.
Deschamps, A. E., S. E. Lallemand, and J. Y. Collot (1998), A detailed study of the Gagua Ridge: A fracture zone uplifted during a plate reorganisation in the Mid-Eocene, *Mar. Geophys. Res.*, *20*(5), 403–423.
Doo, W.-B., S.-K. Hsu, Y.-C. Yeh, C.-H. Tsai, and C.-M. Chang (2015), Age and tectonic evolution of the northwest corner of the West Philippine Basin, *Mar. Geophys. Res.*, *36*(2–3), 113–125.
Eakin, D. H., K. D. McIntosh, H. J. A. Van Avendonk, and L. Lavier (2015), New geophysical constraints on a failed subduction initiation: The structure and potential evolution of the Gagua Ridge and Huatung Basin, *Geochem. Geophys. Geosyst.*, *16*, 380–400, doi:10.1002/2014GC005548.
Engdahl, E. R., R. van der Hilst, and R. Buland (1998), Global teleseismic earthquake relocation with improved travel times and procedures for depth determination, *Bull. Seismol. Soc. Am.*, *88*(3), 722–743.
Fujiwara, T., et al. (1995), Morphological studies of the Ayu Trough, Philippine Sea–Caroline Plate boundary, *Geophys. Res. Lett.*, *22*(2), 109–112.
Gutscher, M. A., F. Klingelhoefer, T. Theunissen, W. Spakman, T. Berthet, T. K. Wang, and C. S. Lee (2016), Thermal modeling of the SW Ryukyu forearc (Taiwan): Implications for the seismogenic zone and the age of the subducting Philippine Sea Plate (Huatung Basin), *Tectonophysics*, *692*, 131–142.
Hall, R. (2002), Cenozoic geological and plate tectonic evolution of SE Asia and the SW Pacific: Computer-based reconstructions, model and animations, *J. Asian Earth Sci.*, *20*(4), 353–431.

Hall, R., and W. Spakman (2015), Mantle structure and tectonic history of SE Asia, *Tectonophysics*, *658*, 14–45.
Hall, R., J. R. Ali, C. D. Anderson, and S. J. Baker (1995a), Origin and motion history of the Philippine Sea Plate, *Tectonophysics*, *251*(1–4), 229–250.
Hall, R., M. Fuller, J. R. Ali, and C. D. Anderson (1995b), The Philippine Sea Plate: Magnetism and reconstructions, in *Geophysical Monograph Series*, vol. 88, pp. 371–404, AGU, Washington, D. C.
Hilde, T., and C. S. Lee (1984), Origin and evolution of the West Philippine Basin—A new interpretation, *Tectonophysics*, *102*(1–4), 85–104.
Hsu, S.-K., Y.-C. Yeh, J.-C. Sibuet, W.-B. Doo, and C.-H. Tsai (2013), A mega-splay fault system and tsunami hazard in the southern Ryukyu subduction zone, *Earth Planet. Sci. Lett.*, *362*, 99–107.
Huang, Z., D. Zhao, A. Hasegawa, N. Umino, J.-H. Park, and I.-B. Kang (2013), Aseismic deep subduction of the Philippine Sea plate and slab window, *J. Asian Earth Sci.*, *75*, 82–94.
International Seismological Centre (2016), *On-line Bulletin*, International Seismological Centre, Thatcham, U. K.
Karig, D. E. (1972), Remnant Arcs, *Geol. Soc. Am. Bull.*, *83*(4), 1057–1068.
Kennett, B. L. N., E. R. Engdahl, and R. Buland (1995), Constraints on seismic velocities in the Earth from traveltimes, *Geophys. J. Int.*, *122*(1), 108–124.
Kuo, B.-Y., W.-C. Chi, C.-R. Lin, E. T.-Y. Chang, J. Collins, and C.-S. Liu (2009), Two-station measurement of Rayleigh-wave phase velocities for the Huatung basin, the westernmost Philippine Sea, with OBS: Implications for regional tectonics, *Geophys. J. Int.*, *179*(3), 1859–1869.
Lallemand, S. (2016), Philippine Sea Plate inception, evolution, and consumption with special emphasis on the early stages of Izu-Bonin-Mariana subduction, *Progress Earth Planet. Sci.*, *3*(1), 15.
Lallemand, S., Y. Font, H. Bijwaard, and H. Kao (2001), New insights on 3-D plates interaction near Taiwan from tomography and tectonic implications, *Tectonophysics*, *335*(3–4), 229–253.
Lallemand, S., T. Theunissen, P. Schnürle, C.-S. Lee, C.-S. Liu, and Y. Font (2013), Indentation of the Philippine Sea plate by the Eurasia plate in Taiwan: Details from recent marine seismological experiments, *Tectonophysics*, *594*, 60–79.
Lallemand, S. E., C.-S. Liu, and Y. Font (1997), A tear fault boundary between the Taiwan orogen and the Ryukyu subduction zone, *Tectonophysics*, *274*(1–3), 171–190.
Li, C., and R. D. van der Hilst (2010), Structure of the upper mantle and transition zone beneath Southeast Asia from traveltime tomography, *J. Geophys. Res.*, *115*, B07308, doi:10.1029/2009JB006882.
Li, C., R. D. van der Hilst, E. R. Engdahl, and S. Burdick (2008), A new global model for *P* wave speed variations in Earth's mantle, *Geochem. Geophys. Geosyst.*, *9*, Q05018, doi:10.1029/2007GC001806.
Lin, J.-Y., S.-K. Hsu, and J.-C. Sibuet (2004), Melting features along the Ryukyu slab tear, beneath the southwestern Okinawa Trough, *Geophys. Res. Lett.*, *31*, L19607, doi:10.1029/2004GL020862.
Lin, J.-Y., S.-K. Hsu, J.-C. Sibuet, C.-S. Lee, and C.-W. Liang (2013), Plate tearing in the northwestern corner of the subducting Philippine Sea Plate, *J. Asian Earth Sci.*, *70–71*, 1–7.
Lister, G., B. Kennett, S. Richards, and M. Forster (2008), Boudinage of a stretching slablet implicated in earthquakes beneath the Hindu Kush, *Nat. Geosci.*, *1*(3), 196–201.
Lister, G. S. (2017a), *Pplates*, Mac OS computer program, ANU, Canberra.
Lister, G. S. (2017b), *eQuakes*, Mac OS computer program, ANU, Canberra.
Lister, G. S., L. T. White, S. Hart, and M. A. Forster (2012), Ripping and tearing the rolling-back New Hebrides slab, *Aust. J. Earth Sci.*, *59*(6), 899–911.
Mahony, S. H., L. M. Wallace, M. Miyoshi, P. Villamor, R. S. J. Sparks, and T. Hasenaka (2011), Volcano-tectonic interactions during rapid plate-boundary evolution in the Kyushu region, SW Japan, *Geol. Soc. Am. Bull.*, *123*(11–12), 2201–2223.
Miller, M. S., A. Gorbatov, and B. L. N. Kennett (2006), Three-dimensional visualization of a near-vertical slab tear beneath the southern Mariana arc, *Geochem. Geophys. Geosyst.*, *7*, Q06012, doi:10.1029/2005GC001110.
Moresi, L., P. G. Betts, M. S. Miller, and R. A. Cayley (2014), Dynamics of continental accretion, *Nature*, *508*(7495), 245–248.
Mrozowski, C. L., S. D. Lewis, and D. E. Hayes (1982), Complexities in the tectonic evolution of the West Philippine Basin, *Tectonophysics*, *82*(1–2), 1–24.
Nakajima, J., and A. Hasegawa (2007), Subduction of the Philippine Sea plate beneath southwestern Japan: Slab geometry and its relationship to arc magmatism, *J. Geophys. Res.*, *112*, B08306, doi:10.1029/2006JB004770.
Nakamura, M. (2004), Crustal deformation in the central and southern Ryukyu Arc estimated from GPS data, *Earth Planet. Sci. Lett.*, *217*(3–4), 389–398.
Obayashi, M., J. Yoshimitsu, and Y. Fukao (2009), Tearing of stagnant slab, *Science*, *324*(5931), 1173–1175.
Okino, K., Y. Shimakawa, and S. Nagaoka (1994), Evolution of the Shikoku Basin, *J. Geomagn. Geoelectr.*, *46*(6), 463–479.
Okino, K., S. Kasuga, and Y. Ohara (1998), A new scenario of the Parece Vela Basin genesis, *Mar. Geophys. Res.*, *20*(1), 21–40.
Peacock, S. M. (2001), Are the lower planes of double seismic zones caused by serpentine dehydration in subducting oceanic mantle?, *Geology*, *29*(4), 299–302.
Pi, J.-L., C.-F. You, and K.-L. Wang (2016), The influence of Ryukyu subduction on magma genesis in the Northern Taiwan Volcanic Zone and Middle Okinawa Trough—Evidence from boron isotopes, *Lithos*, *260*, 242–252.
Rawlinson, N., and W. Spakman (2016), On the use of sensitivity tests in seismic tomography, *Geophys. J. Int.*, *205*(2), 1221–1243.
Richards, S., R. Holm, and G. Barber (2011), When slabs collide: A tectonic assessment of deep earthquakes in the Tonga-Vanuatu region, *Geology*, *39*(8), 787–790.
Rosenbaum, G., M. Gasparon, F. P. Lucente, A. Peccerillo, and M. S. Miller (2008), Kinematics of slab tear faults during subduction segmentation and implications for Italian magmatism, *Tectonics*, *27*(2), TC2008, doi:10.1029/2007TC002143.
Ryan, W. B. F., et al. (2009), Global multi-resolution topography synthesis, *Geochem. Geophys. Geosyst.*, *10*(3), Q03014, doi:10.1029/2008GC002332.
Schnürle, P., C.-S. Liu, S. E. Lallemand, and D. L. Reed (1998), Structural insight into the south Ryukyu margin: Effects of the subducting Gagua Ridge, *Tectonophysics*, *288*(1–4), 237–250.
Sdrolias, M., W. R. Roest, and R. D. Müller (2004), An expression of Philippine Sea plate rotation: The Parece Vela and Shikoku Basins, *Tectonophysics*, *394*(1–2), 69–86.
Seno, T., and S. Maruyama (1984), Paleogeographic reconstruction and origin of the Philippine Sea, *Tectonophysics*, *102*(1–4), 53–84.
Sibuet, J.-C., S.-K. Hsu, X. Le Pichon, J.-P. Le Formal, D. Reed, G. Moore, and C.-S. Liu (2002), East Asia plate tectonics since 15 Ma: Constraints from the Taiwan region, *Tectonophysics*, *344*(1–2), 103–134.
Sigloch, K., N. McQuarrie, and G. Nolet (2008), Two-stage subduction history under North America inferred from multiple-frequency tomography, *Nat. Geosci.*, *1*(7), 458–462.

Spakman, W., and R. Hall (2010), Surface deformation and slab—Interaction during Banda arc subduction rollback, *Nat. Geosci.*, *3*(8), 562–566.
Spakman, W., and G. Nolet (1988), Imaging algorithms, accuracy and resolution in delay time tomography, in *Mathematical Geophysics*, pp. 155–187, Springer, Dordrecht, Netherlands.
Spakman, W., and R. Wortel (2004), A tomographic view on western Mediterranean geodynamics, in *The TRANSMED Atlas. The Mediterranean Region from Crust to Mantle*, pp. 31–52, Springer, Berlin, Heidelberg.
Sternai, P., L. Jolivet, A. Menant, and T. Gerya (2014), Driving the upper plate surface deformation by slab rollback and mantle flow, *Earth Planet. Sci. Lett.*, *405*, 110–118.
Thorkelson, D. J. (1996), Subduction of diverging plates and the principles of slab window formation, *Tectonophysics*, *255*(1–2), 47–63.
van Hinsbergen, D. J. J., P. C. Lippert, G. Dupont-Nivet, N. McQuarrie, P. V. Doubrovine, W. Spakman, and T. H. Torsvik (2012), Greater India Basin hypothesis and a two-stage Cenozoic collision between India and Asia, *Proc. Natl. Acad. Sci. U.S.A.*, *109*(20), 7659–7664.
van Hunen, J., and M. B. Allen (2011), Continental collision and slab break-off: A comparison of 3-D numerical models with observations, *Earth Planet. Sci. Lett.*, *302*(1–2), 27–37.
Wang, Z., R. Huang, J. Huang, and Z. He (2008), *P* wave velocity and gradient images beneath the Okinawa Trough, *Tectonophysics*, *455*(1–4), 1–13.
Watanabe, Y. (2005), Late Cenozoic evolution of epithermal gold metallogenic provinces in Kyushu, Japan, *Miner. Deposita*, *40*(3), 307–323.
Wei, W., J. Xu, D. Zhao, and Y. Shi (2012), East Asia mantle tomography: New insight into plate subduction and intraplate volcanism, *J. Asian Earth Sci.*, *60*, 88–103.
Wei, W., D. Zhao, J. Xu, F. Wei, and G. Liu (2015), *P* and *S* wave tomography and anisotropy in Northwest Pacific and East Asia: Constraints on stagnant slab and intraplate volcanism, *J. Geophys. Res. Solid Earth*, *120*, 1642–1666, doi:10.1002/2014JB011254.
Widiyantoro, S., B. Kennett, and R. D. van der Hilst (1999), Seismic tomography with *P* and *S* data reveals lateral variations in the rigidity of deep slabs, *Earth Planet. Sci. Lett.*, *173*(1–2), 91–100.
Wortel, M. J. R., and W. Spakman (2000), Subduction and slab detachment in the mediterranean-carpathian region, *Science*, *290*(5498), 1910–1917.
Wu, F. T., W. T. Liang, J.-C. Lee, H. Benz, and A. Villaseñor (2009), A model for the termination of the Ryukyu subduction zone against Taiwan: A junction of collision, subduction/separation, and subduction boundaries, *J. Geophys. Res.*, *114*, B07404, doi:10.1029/2008JB005950.
Wu, J., and J. Suppe (2011), Seismic tomographic constraints on plate tectonic reconstructions of the Philippine Sea plate near East Asia, Abstract T42B-08 presented at 2011 Fall Meeting, AGU, San Francisco, Calif.
Wu, J., J. Suppe, R. Lu, and R. Kanda (2016), Philippine Sea and East Asian plate tectonics since 52 Ma constrained by new subducted slab reconstruction methods, *J. Geophys. Res. Solid Earth*, *121*, 4670–4741, doi:10.1002/2016JB012923.
Yamazaki, T., N. Seama, K. Okino, K. Kitada, and J. Naka (2003), Spreading process of the northern Mariana Trough: Rifting-spreading transition at 22 degrees N, *Geochem. Geophys. Geosyst.*, *4*(9), 1075, doi:10.1029/2002GC000492.
Zhao, D., T. Yanada, A. Hasegawa, N. Umino, and W. Wei (2012), Imaging the subducting slabs and mantle upwelling under the Japan Islands, *Geophys. J. Int.*, *190*(2), 816–828.